Molecules **2015**, *20*, 5638-5666; doi:10.3390/molecules20045638

OPEN ACCESS

molecules

ISSN 1420-3049

www.mdpi.com/journal/molecules

Review

Nanoporous Materials as New Engineered Catalysts for the Synthesis of Green Fuels

Ioana Fechete [1,*] and Jacques C. Vedrine [2,*]

[1] Institut de Chimie et Procédés pour l'Energie, l'Environnement et la Santé—ICPEES, UMR 7515 CNRS, Université de Strasbourg, 25 rue Becquerel, 67087 Strasbourg Cedex 2, France

[2] Laboratoire de Réactivité de Surface, UMR-CNRS 7197, Université P. & M. Curie-Paris 06, Sorbonne Universités, 4 Place Jussieu, 75252 Paris, France

* Authors to whom correspondence should be addressed; E-Mails: ifechete@unistra.fr (I.F.); jacques.vedrine@upmc.fr (J.C.V.); Tel.: +33-0-368852756 (I.F.); +33-0-668536212 (J.C.V.); Fax: +33-0-368852761 (I.F.); +33-0-144276510 (J.C.V.).

Academic Editor: Geoffrey L. Price

Received: 4 February 2015 / Accepted: 23 March 2015 / Published: 31 March 2015

Abstract: This review summarizes the importance of nanoporous materials and their fascinating structural properties with respect to the catalytic and photocatalytic reduction of CO_2 to methane, toward achieving a sustainable energy supply. The importance of catalysis as a bridge step for advanced energy systems and the associated environmental issues are stressed. A deep understanding of the fundamentals of these nanoporous solids is necessary to improve the design and efficiency of CO_2 methanation. The role of the support dominates the design in terms of developing an efficient methanation catalyst, specifically with respect to ensuring enhanced metal dispersion and a long catalyst lifetime. Nanoporous materials provide the best supports for Ni, Ru, Rh, Co, Fe particles because they can prevent sintering and deactivation through coking, which otherwise blocks the metal surface as carbon accumulates. This review concludes with the major challenges facing the CO_2 methanation by nanoporous materials for fuel applications.

Keywords: zeolites; mesoporous materials; methane; Synthetic Natural Gas (SNG); Ni nanoparticles; deactivation prevention

1. Introduction

Energy generated via renewable energy strategies is critical to various aspects of global human development, including harmony, equity, employment, ecosystems, and environmental protection. As the demand for energy continues to increase worldwide, mainly in emerging economies, overcoming energy barriers is a key step in the continued development of civilization. Modern economic development (chemical industry, power plants, transportation sector) is inherently dependent on fossil fuels, which are non-renewable energy sources [1–5], yet fossil fuels still represent more than 85% of the world energy consumption. Since the industrial revolution in the 19th century, the majority of anthropogenic CO_2 emissions have been attributed to the consumption of fossil fuels [6–12], resulting in environmental pollution and very probably in increased global warming effect. In this context, a challenge for 21st century is the control of technological processes, developing highly active and selective reaction systems with atom efficiency and minimizing unwanted secondary reactions [13–22]. Excessive CO_2 emissions have caused global climate change and increased planetary temperatures; more specifically, the global surface temperature has increased by 0.74 °C over the past century. The CO_2 levels in the earth atmosphere have increased significantly by more than 10 billion tonnes per year. Moreover, heavy dependence on fossil fuels causes problems in energy security because a large fraction of the fossil fuel consumed is imported, and these resources are non-renewable. Therefore, sustainable energy production, combined with moderate consumption practices, represents a challenge to our civilization [1,2,4,5,23–25]. Alternative energy sources should be derived from geothermal, hydrothermal, solar, wind, nuclear and other renewable resources. One perspective is that all sectors should employ low-pollution renewable energy with the net "zero emission" of CO_2. However, several petrochemical companies are considering biomass and natural gas fuel sources as alternative renewable feedstocks.

Several strategies should be considered to reduce the amount of carbon dioxide emitted into the atmosphere. Examples include the implementation of new green technologies by exchanging the fossil fuels for renewable energy sources, the biological, physical and chemical capture and storage of CO_2, and the conversion of CO_2 to various chemical products and fuels as shown in Figure 1 [2,4,11,12,21,24,26].

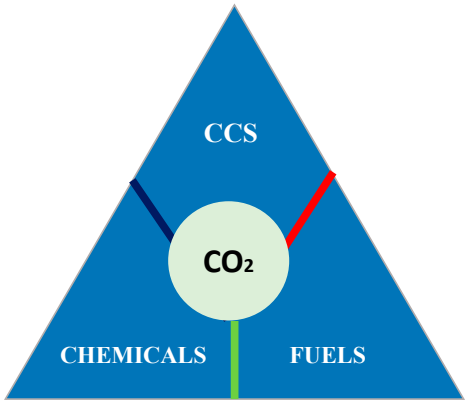

Figure 1. Possible strategies of reducing CO_2.

Carbon capture and storage (CCS) has received major attention in recent years [27–32]. In this strategy, several approaches have been tested for the removal of CO_2 from power plants or other large

emitters. These approaches include amine scrubbing, cryogenic distillation, membrane separation and the use of an absorbent/adsorbent [33]. Amine scrubbing is inconvenient in that this approach is inherently corrosive and there exists difficulty in solvent regeneration. In comparison, cryogenic distillation imposes a high energetic demand. Membrane separation is limited by permeability-selectivity. In contrast, the adsorption of CO_2 into nanoporous materials is both an energy efficient process and offers separation capability. Several nanoporous adsorbents have been tested for CO_2 capture [33]. Among these nanoporous materials, the zeolites and MOF have predominantly been studied, both of which present high selectivities for the separation of flue gas. The high selectivity of these materials has been explained by the zeolite electric field, which inherently varies in strength, further suggesting that the architecture of the zeolite structure is a very important feature [34–36]. These nanoporous materials have been suggested as suitable materials for CO_2/CH_4 separation. In the CCS approach, CO_2 is captured in either a pre- or post-combustion process. In pre-combustion capture, the partial oxidation of a feedstock fuel produces syngas, which reacts with steam to yield shifted syngas. In the post-combustion capture process, the CO_2 is separated from the exhaust flue gas, which primarily consists of N_2 and CO_2 [34–36]. The captured CO_2 is then stored either in the deep ocean or underground in geological formations such as depleted oil and gas reservoirs. The problem there is that CO_2 should be inert chemically with respect to the geological rocks, in presence of water and for a very long time. Although the implementation of CSS will lead to decreased emissions of CO_2 into the atmosphere and will yield raw materials, implementation with respect to the world economy is an inconvenient aspect of this approach. For CCS, the sequestration site must be near the CO_2 source. Often, the CO_2 must eventually be transported to a different site, which necessitates further investment for the development of adequate infrastructure. A plausible alternative CCS strategy is the development of a new catalytic process or improvements to those already in existence for the use of captured carbon as a reagent to produce useful chemicals or fuel.

The conversion of CO_2 should be used as an alternative to petrochemistry and petrorefineries and as a bridging technology toward the development of a sustainable energy supply, and consequently sustainable industrial development, for the long term [37]. However, the process of CO_2 valorization by conversion into chemical products has been known for many decades; more specifically, the synthesis of salicylic acid was discovered in 1969 [2,38], the synthesis of $NaHCO_3$–Na_2CO_3 was developed in 1882 and was known as the "Solvay process" [39] and the synthesis of urea was identified in 1922 [40]. In 1970 [2], the catalytic conversion of CO_2 to synthesize methanol from syngas enriched with CO_2 was first developed. The valorization of CO_2 by conversion into other chemicals has been discussed in several reviews [2,3,11,12,24]. A promising approach for the valorization of CO_2 was the catalytic conversion of CO_2 into fuels: Fischer-Tropsch, MeOH, DME, CH_4 (synthetic natural gas—SNG), and syngas.

In this review, we focus only on CO_2 methanation for the SNG process. Methanation involves the catalytic hydrogenation of carbon oxides to provide an efficient alternative to conventional natural gas [41]; moreover, the infrastructure for handling CH_4 is well established. SNG is considered a promising approach for obtaining this valuable, high-combustion-efficiency gaseous fuel which can be used in current hydrocarbon-based automobiles and transportation systems while reducing dependence on petroleum; in addition, this fuel is considered environmentally friendly as it recovers CO_2 used as reactant in its synthesis [42–46]. Catalysis is a core technology of the energy industry [47–51] with an important role in the area production of sustainable fuels and energy [4,5,52–58]. The development of suitable catalysts for the conversion of CO_2 is under intensive study by researchers around the world. A

large number of excellent studies on various metal catalysts have appeared in the literature [59–63], and supported nickel catalysts are the most widely studied for CO_2 methanation due to their high ability to dissociate CO_2 [64,65]. Their higher activities and selectivities for methane have been attributed to various factors, including the nature of the support, nature of the metal, amount of metal and its dispersion. However, these traditional catalysts suffer from several drawbacks, including sensitivity to metal site poisoning, sintering, coke deposition, and deactivation [66–70]. In light of the ubiquitous restrictions imposed by environmental legislation and economics, the use of nanostructured porous catalysts, which can be very selective for the desired products, is one alternative to the use of traditional catalysts [71,72]. Nanoporous catalysts are of great interest because of their highly ordered pore structure, high specific surface area, and tailorable pore size, framework, and surface properties [73–82]. Nanoporous materials can be used as hosts for the preparation of nano-sized catalysts. The advantages of the small metal particles of nanoporous catalyst are a great variety in the valence band electron structure, short range ordering, enhanced interaction with the environment due to the high number of dangling bonds, and self-structuring for optimum performance in chemisorption. Surface area is the main factor which controls the catalytic activity of a nanoporous catalyst. The surface area of a porous material is higher than the surface of a non-porous material. The large surface area leads to a well-distributed dispersion of the catalytic phase at high loadings; this can hardly be achieved with non-porous traditional support, such as silica gel or alumina. The uniform porosity results in monodispersed nanometer-sized catalysts. In cases where catalytic activity is size-sensitive, it is very desirable to use nanochannels as a confinement zone to obtain the nanocatalyst. Taking into account that the catalytic reactions occur on surface of the catalysts, the higher surface leads to an improved activity and selectivity. One of crucial points is whether turnover frequency measured for a given catalytic reaction increases or decreases as the particle size is diminished.

Nanoporous catalysts play an important role in all areas of catalysis, especially in energy and environmental applications [83–91]. The structural aspects of nanoporous materials have been summarized in several excellent publications [73,92–98]. Therefore, a meaningful assessment of the importance of nanoporous catalysts over time should be performed. This review comprehensively discusses the catalytic and photocatalytic conversion of CO_2 to CH_4 and the role of nanoporous catalysts in these reactions.

2. Thermodynamics of CO_2

CO_2 is kinetically and thermodynamically stable and the methanation reaction is extremely exothermic due to the high concentration of oxidized carbon forms in the feed gas [99]. The chemical reactions are driven by the difference between the Gibbs free energy values of the reactants and products of the chemical reaction, as shown by the Gibbs–Helmholtz equation: $\Delta G° = \Delta H° - T\Delta S°$. A large energy input, optimized reaction conditions and active catalysts are necessary to transform CO_2 into useful products. This is because CO_2 is inert: the carbon atom in CO_2 is in its most oxidized state, which means that its chemical transformation is thermodynamically highly unfavorable [100]. In this case, as a raw material, CO_2 is in its lowest energy state, constituting a major obstacle in the establishment of industrial processes for CO_2 conversion.

Upon analyzing the Gibbs free energy of the exothermic hydrogenation of CO_2, a majority of the associated reactions are found to be thermodynamically unfavorable. Because the Gibbs free energy values are more positive than the corresponding $\Delta H°$ values, they are less favorable; only a few reactions

have both negative ΔG° and ΔH° values. Values of ΔG < 0 correspond to hydrogenation or reactions with products containing C-O bonds. Favorable values of ΔG in the hydrogenation reaction are associated with the formation of water. Because hydrogen must be produced at the cost of the input energy, none of these reactions is favorable for CO_2 mitigation.

The values of the enthalpy and Gibbs free energy, calculated by ASPEN software [3,101–103], of the exothermic, ΔH < 0, reaction in the CO_2 hydrogenations are as follows:

$$CO_{2(g)} + H_{2(g)} \rightarrow HCOOH_{(l)};\ \Delta H° = -31.0\ kJ\cdot mol^{-1};\ \Delta G° = +34.3\ kJ\cdot mol^{-1} \quad (1)$$

$$CO_{2(g)} + 2H_{2(g)} \rightarrow HCHO_{(g)} + H_2O_{(l)};\ \Delta H\ ° = -11.7\ kJ\cdot mol^{-1};\ \Delta G° = +46.6\ kJ\cdot mol^{-1} \quad (2)$$

$$CO_{2(g)} + 3H_{2(g)} \rightarrow CH_3OH_{(l)} + H_2O_{(l)};\ \Delta H° = -137.8\ kJ\cdot mol^{-1};\ \Delta G° = -10.7\ kJ\cdot mol^{-1} \quad (3)$$

$$CO_{2(g)} + 4H_{2(g)} \rightarrow CH_{4(g)} + 2H_2O_{(l)};\ \Delta H° = -259.9\ kJ\cdot mol^{-1};\ \Delta G° = -132.4\ kJ\cdot mol^{-1} \quad (4)$$

$$2CO_{2(g)} + H_{2(g)} \rightarrow (COOH)_{2(l)};\ \Delta H° = -39.3\ kJ\cdot mol^{-1};\ \Delta G° = 85.3\ kJ\cdot mol^{-1} \quad (5)$$

$$2CO_{2(g)} + 6H_{2(g)} \rightarrow CH_3OCH_{3(g)} + 3H_2O_{(l)};\ \Delta H° = -264.9\ kJ\cdot mol^{-1};\ \Delta G° = -38.0\ kJ\cdot mol^{-1} \quad (6)$$

$$CO_{2(g)} + H_2 + CH_3OH_{(l)} \rightarrow HCOOCH_{3(l)} + H_2O_{(l)};\ \Delta H° = -31.8\ kJ\cdot mol^{-1};\ \Delta G° = -25.8\cdot kJ\ mol^{-1} \quad (7)$$

$$CO_{2(g)} + H_2 + CH_3OH_{(l)} \rightarrow CH_3COOH_{(l)} + H_2O_{(l)};\ \Delta H° = -135.4\ kJ\cdot mol^{-1};\ \Delta G° = -63.6\ kJ\cdot mol^{-1} \quad (8)$$

$$CO_{2(g)} + 3H_{2(g)} + CH_3OH_{(l)} \rightarrow C_2H_5OH_{(l)} + 2H_2O_{(l)};\ \Delta H° = -221.6\ kJ\cdot mol^{-1};\ \Delta G° = -88.9\ kJ\cdot mol^{-1} \quad (9)$$

$$CO_{2(g)} + H_{2(g)} + NH_{3(g)} \rightarrow HCONH_{2(l)} + H_2O_{(l)};\ \Delta H° = -103.0\ kJ\cdot mol^{-1};\ \Delta G° = +7.2\ kJ\cdot mol^{-1} \quad (10)$$

$$CO_{2(g)} + CH_{4(g)} \rightarrow CH_3COOH_{(l)};\ \Delta H° = -13.3\ kJ\cdot mol^{-1};\ \Delta G° = +58.1\ kJ\cdot mol^{-1} \quad (11)$$

$$CO_{2(g)} + CH_{4(g)} + H_{2(g)} \rightarrow CH_3CHO_{(l)} + H_2O_{(l)};\ \Delta H° = -14.6\ kJ\cdot mol^{-1};\ \Delta G° = +74.4\ kJ\cdot mol^{-1} \quad (12)$$

$$CO_{2(g)} + CH_{4(g)} + 2CO_{2(g)} \rightarrow (CH_3)_2CO_{(l)} + H_2O_{(l)};\ \Delta H° = -70.5\ kJ\cdot mol^{-1};\ \Delta G° = +51.2\ kJ\cdot mol^{-1} \quad (13)$$

$$CO_{2(g)} + C_2H_{2(g)} + H_{2(g)} \rightarrow CH_2 = CHCOOH_{(l)};\ \Delta H° = -223.6\ kJ\cdot mol^{-1};\ \Delta G° = -115.0\ kJ\cdot mol^{-1} \quad (14)$$

$$CO_{2(g)} + C_2H_{4(g)} \rightarrow CH_2 = CHCOOH_{(l)};\ \Delta H° = -49.1\ kJ\cdot mol^{-1};\ \Delta G° = +26.2\ kJ\cdot mol^{-1} \quad (15)$$

$$CO_{2(g)} + C_2H_{4(g)} + H_{2(g)} \rightarrow C_2H_5COOH_{(l)};\ \Delta H° = -166.6\ kJ\cdot mol^{-1};\ \Delta G° = -56.6\ kJ\cdot mol^{-1} \quad (16)$$

$$CO_{2(g)} + C_2H_{4(g)} + 2H_{2(g)} \rightarrow C_2H_5CHO + H_2O_{(l)};\ \Delta H° = -171.1\ kJ\cdot mol^{-1};\ \Delta G° = -44.4\ kJ\cdot mol^{-1} \quad (17)$$

$$CO_{2(g)} + C_6H_{6(l)} \rightarrow C_6H_5COOH_{(l)};\ \Delta H° = -21.6\ kJ\cdot mol^{-1};\ \Delta G° = +30.5\ kJ\cdot mol^{-1} \quad (18)$$

$$CO_{2(g)} + C_6H_5OH_{(l)} \rightarrow mC_6H_4(OH)COOH_{(l)};\ \Delta H° = -6.6\ kJ\cdot mol^{-1};\ \Delta G° = +46.9\ kJ\cdot mol^{-1} \quad (19)$$

Hydrogenation reactions of CO_2 with $\Delta H > 0$ can be performed [3,101–103]. These reactions are associated with highly positive $\Delta G°$ values and are not favorable.

$$CO_{2(g)} + CH_2{=}CH_{2(g)} \rightarrow CH_2CH_2O_{(l)} + CO_{(g)};\ \Delta H° = +152.9\ kJ{\cdot}mol^{-1};\ \Delta G° = +177.3\ kJ{\cdot}mol^{-1} \quad (20)$$

$$CO_{2(g)} + C(s) \rightarrow 2CO_{(g)};\ \Delta H° = +172.6\ kJ{\cdot}mol^{-1};\ \Delta G° = +119.9\ kJ{\cdot}mol^{-1} \quad (21)$$

$$3CO_{2(g)}\ CH_{4(g)} \rightarrow 4CO_{(g)} + 2H_2O_{(l)};\ \Delta H° = +235.1\ kJ{\cdot}mol^{-1};\ \Delta G° = +209.2\ kJ{\cdot}mol^{-1} \quad (22)$$

$$CO_{2(g)} + CH_{4(g)} \rightarrow 2CO_{(g)} + 2H_{2(g)};\ \Delta H° = +247.5\ kJ{\cdot}mol^{-1};\ \Delta G° = +170.8\ kJ{\cdot}mol^{-1} \quad (23)$$

$$CO_{2(g)} + 2CH_{4(g)} \rightarrow C_2H_{6(g)} + CO_{(g)} + H_2O_{(l)};\ \Delta H° = +58.8\ kJ{\cdot}mol^{-1};\ \Delta G° = +88.0\ kJ{\cdot}mol^{-1} \quad (24)$$

$$2CO_{2(g)} + 2CH_{4(g)} \rightarrow C_2H_{4(g)} + 2CO_{(g)} + 2H_2O_{(l)};\ \Delta H° = +189.7\ kJ{\cdot}mol^{-1};\ \Delta G° = +208.3\ kJ{\cdot}mol^{-1} \quad (25)$$

$$CO_{2(g)} + C_2H_{4(g)} \rightarrow C_2H_4O_{(g)} + CO_{(g)};\ \Delta H° = +178.0\ kJ{\cdot}mol^{-1};\ \Delta G° = +176.0\ kJ{\cdot}mol^{-1} \quad (26)$$

In general, the conversion of CO_2 is accompanied by the production of CO. The reaction enthalpies for the production of the same product from either CO or CO_2 are comparable, although in most cases, CO is favored compared to CO_2 [3,101–103].

3. Reaction Mechanism of CO_2 Methanation

Over the past few decades, understanding the mechanism of the methanation of CO_2 has represented a significant challenge. Following a careful analysis of several studies, we ascertained that in the methanation of CO_2, two types of mechanisms occur: with CO as intermediate (Figure 2), when CO_2 in converted to CO before the methanation [104–108] and direct methanation of CO_2 (Figure 2) without forming CO as intermediate [109,110].

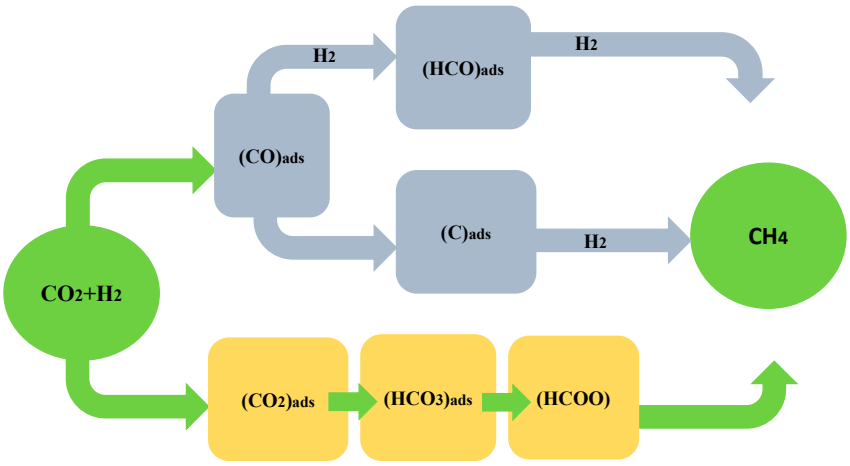

Figure 2. Reaction mechanisms of CO_2 methanation.

3.1. Methanation of CO_2 with CO as Intermediate

As a function of the nature and history of catalysts and their reaction conditions, this reaction mechanism is difficult to establish, taking into account that in the literature on CO_2 methanation, it is believed [104–108,111] that carbon monoxide is a critical intermediate in carbon dioxide methanation.

More specifically, the methanation of CO_2 consists of the reduction of CO_2 to CO: $CO_2 + H_2 \leftrightarrow CO + H_2O$ followed by the conversion of CO into methane (or other alkanes); $CO + 3H_2 \leftrightarrow CH_4 + H_2O$. In this case, the mechanism is identical to that for CO methanation [112,113]. Because the equilibrium for $CO_2 + H_2 \leftrightarrow CO + H_2O$ is somewhat unfavorable at the reaction temperatures (200–400 °C), it can be noted that this reaction path is unlikely. One way to circumvent this difficulty is to require that at these temperatures the methanation of carbon monoxide: $CO + 3H_2 \leftrightarrow CH_4 + H_2O$, proceed at significantly faster rates than carbon monoxide production. If carbon monoxide were consumed as rapidly as it forms, no carbon monoxide would be observed in the reactor exit stream [114]. Another mechanism, first suggested by Doehlemann [115] in 1938 and subsequently by Kul'kowa and coworkers [116,117], was also described by Wagner [118]. In this alternative mechanism [118], CO_2 dissociates into $CO_{(ad)}$ and $O_{(ad)}$, ($CO_{2\ (ad)} \rightarrow CO_{(ad)} + O_{(ad)}$) and the adsorbed oxygen atoms react with molecular hydrogen in a single step ($H_{2(g)} + O_{(ad)} \rightarrow H_2O_{(ad)}$), forming water, while the adsorbed CO is transformed into methane ($CO_{(ad)} \rightarrow CH_4$). However, this mechanism assumes that the $H_{2(g)} + O_{(ad)} \rightarrow H_2O_{(ad)}$ step is rate-controlling of CO_2 methanation. In the methanation of CO_2 on Rh/Al_2O_3 [119], the dissociation of CO_2 into carbon monoxide and oxygen on the surface of the catalysts was also observed in diffuse reflectance infrared Fourier transform (DRIFT) studies. The Rh–CO (2048 cm^{-1}), Rh^{3+}–CO (2123 cm^{-1}), and Rh–$(CO)_2$ (2024 and 2092 cm^{-1}) bands confirmed the formation of CO_{ads}. CO_2 adsorbed as Rh–$(CO)_2$ and CO associated with oxidized Rh are the most hydrogen-reactive species. The presence of CO as a key intermediate in the methanation of CO_2 was proved by steady-state transient (SST) studies on a Ru/TiO_2 catalyst [107]. However, at the interface between the metal and support, the presence of formate as a result of reaction with carbonate species was also observed, as an intermediate for the formation of CO. Single crystals of Ni have been suggested as a model catalyst for CO_2 methanation [120,121]. The dissociation of CO_2 on Ni(100) [106] proved that CO_2 is first converted to CO and subsequently to carbon before hydrogenation. The authors observed that the activation energy and reaction rate for CO_2 methanation are very close to the values for the formation of CH_4 (88.7 $kJ \cdot mol^{-1}$) from CO (72.8–82.4 $kJ \cdot mol^{-1}$) under identical reaction conditions. It is known also that the formed CO is then dissociated into C and O atoms on the metal sites before being further hydrogenated into methane by the dissociated H_2 that remains on the metal particles [105,122]. When a Ni(111) surface was tested using atom superposition and electron delocalization-molecular orbital theory [123], the dissociation of CO was found to be the rate-determining step. However, the elementary steps of the CO_2 methanation reaction consisted of two mechanisms, carbon formation and carbon methanation. For the first mechanism, the activation energies were calculated to be 1.27 eV (~120 kJ^{-1}) for CO_2 dissociation, 2.97 eV (~290 $kJ \cdot mol^{-1}$) for CO dissociation, and 1.93 eV (~190 $kJ \cdot mol^{-1}$) for 2CO dissociation. For the carbon methanation mechanism, the following activation energies were reported: 0.72 eV (~72 $kJ \cdot mol^{-1}$) for methylidyne, 0.52 eV (~50 $kJ \cdot mol^{-1}$) for methylene, and 0.50 eV (~48 $kJ \cdot mol^{-1}$) for methane [123].

3.2. Methanation of CO_2 without CO as Intermediate

Elsewhere, the direct methanation of CO_2 without CO as an intermediate has also been reported [109,110]. An alternative mechanism for CO_2 methanation on various catalysts consists of the methanation of CO_2 through carbonates and formates, which are directly hydrogenated into CH_4 [107,108,124–127]. The CO_2 is first dissociated into CO directly [128–130]. CO_2 methanation on Pd–MgO/SiO_2 catalysts [126] has shown

that the MgO support initiates the reaction. In this case, magnesium carbonate species were observed on the surface of the catalysts. Pd, the active phase of the catalysts, dissociates molecular hydrogen and promotes the hydrogenation of the carbonates and residual carbon atoms [131]. These results show the synergy between the basic support and the active phase. CO_2, which is an acidic molecule, is activated by the basic sites of the MgO support to form magnesium carbonate, while the metallic sites of Pd dissociate the hydrogen. However, methoxy groups were also observed in the CO methanation mechanism [132]. A Ni/CeO_2 catalyst showed the highest CO_2 conversions at lower temperatures with CH_4 selectivities very close to 100% [133–135]. The better performance of CeO_2 support was attributed to its higher ability to adsorb CO_2 molecules, followed by its ability to reduce the molecules into CO and then convert the CO into CH_4. Temperature-programmed reduction (TPR) experiments on Ru catalysts [59] have shown that CO + H_2 reacts to produce CO_2 and water, without the production of methane; therefore, gaseous phase CO is not a reaction intermediate during CO_2 methanation with $Ce_{0.95}Ru_{0.05}O_2$ catalyst [59]. Moreover, CO_2 was converted directly into methane, without CO as intermediate when nanoporous gallium oxide was used in the photocatalytic conversion of carbon dioxide into methane [136].

4. Catalytic Conversion of CO_2 to CH_4

The Sabatier reaction, discovered in 1902 by Sabatier and Senderens [137], consists of the catalytic hydrogenation of carbon dioxide to methane. This methanation reaction was investigated by NASA as a necessity for reclaiming oxygen within closed-cycle life support systems. In this case, CO_2 from the cabin atmosphere is transformed into water vapor, which is electrolyzed and used to return oxygen to the cabin, in addition to one part of hydrogen, as required by the Sabatier reaction. The other part of hydrogen is provided from the electrolysis of stored water, which produces breathable oxygen as a by-product, reducing the proportion of available carbon dioxide that must be reacted and assuring excess carbon dioxide in the feed mixture. In the 1970s, the direct hydrogenation of highly thermodynamically stable CO_2 attracted significant attention for the production of substitute natural gas (SNG), due to the shortage of natural gas at that time [138]. The ever-increasing demand for natural gas as a fuel and raw material has stimulated renewed efforts to find other means of methane production. With mounting evidence of an "energy crisis" upon us, alternative approaches such as catalytically synthesizing methane from hydrogen and carbon dioxide continue to meet with increased promise for development.

The CO_2 methanation reaction is reversible and highly exothermic $CO_{2(g)} + 4H_{2(g)} \rightarrow CH_{4(g)} + 2H_2O_{(l)}$, $\Delta H° = -259.9$ kJ·mol^{-1}, $\Delta G° = -132.4$ kJ·mol^{-1}. Because the highly oxidized CO_2 molecule is highly thermodynamically stable, this compound is not reactive. In this case, CO_2 methanation requires high-energy substances and entails an eight-electron process with kinetic limitations [131,139]. However, when a reactive catalyst is used, the reaction takes place at low temperatures with high yields and selectivities [131,139]. Porous materials such as microporous zeolite and mesoporous materials have been used for CO_2 hydrogenation; even so, CO_2 methanation over zeolites has been investigated less extensively than the hydrogenation of CO. The active phase deposited on the support has been investigated using a number of catalytic systems.

The catalysts used in CO_2 methanation include the transition elements Ni [106,122,127,140–146], Pd [147], Pt [148], Co [149–151], Rh [66,152–154], Mg [155], Zn [156], Zr [157,158], Sn [159], U [160], Ta [161], Nb [162], Cr [163], Ir [164,165], Cu [166], Ag [166], V [167], W [163,168–170],

Mo [171–173], Mn [174,175], Ti [176,177], Fe [72,178–181]. Excellent reviews of these reports have also been published. Among these metals, Ni, Ru and Rh have been the most effective in this reaction [59,71,104,182–185]. Ru and Rh have been reported as the most selective toward methane [59,104,184], while Ni has been the most-studied catalyst [71,182] because it presents high activity and selectivity, is cheaper, and hence more interesting from a commercial perspective. Ni has been dispersed on several support types with acidic, basic or neutral sites; in these studies, it was concluded that the activity, selectivity and stability of catalysts made with Ni is determined by the nature of the support. Different interactions can be established between the metal and the support, and these differences influence the catalytic properties of the active metal sites [182]. In spite of the large number of studies performed on Ni-supported catalysts, Ni/Al_2O_3 is the best-known catalyst for industrial CO_2 methanation applications worldwide and it has been commercialized by Evonik, Johnson Matthey, Topsoe and Clariant-Sud Chemie.

The Raney catalysts are very well known in the hydrogenation industry and seem to present high reactivity and selectivity during CO_2 methanation [186]. Both of these properties have been attributed to the catalyst's high surface area and structural/thermal properties. The amount of Ni used is also very important because Ni leads to higher methane selectivity [187]. The high activity of Ni/Al_2O_3 catalysts in such applications is partially attributed to the presence of a nickel aluminate spinel phase, located at the metal-support interface, which is thought to stabilize the metal particles. Concurrently, it is believed that the formation of a nickel aluminate spinel phase also results in inefficiencies when using Ni-based catalysts [188,189]. Ni/Al_2O_3 catalysts prepared through impregnation delivered a rapid deactivation process during an exothermic methanation reaction, resulting in the sintering of Ni particles and severe carbon deposition [190]. Furthermore, the most commonly reported problem associated with Ni-based catalysts is deactivation at low temperatures, due to the interaction of the metal particles with CO and the formation of mobile/volatile nickel carbonyls that lead to the sintering of the metal particles [191,192]. To overcome the problems associated with deactivation and sintering, several solutions have been proposed. As it is commonly known in catalysis chemistry, the addition of a second metal such La, Ce, Sm, Fe, Mg, Y, Pt, Ru, Rh and/or the use of a porous support such as a zeolite or a mesoporous material can be used to inhibit metal sintering [193–196]. The catalyst containing nanoporous solids is very selective to methane without CO formation. The presence of either the second metal species or the porous structure of the support, which provides a high surface area, can prevent sintering and increase the dispersion of metal particles. For example, when using Al_2O_3 or SiO_2 supports with Ni or Ru metal, the addition of CeO_2 improves the activity of the system for CO_2 methanation [134,197,198]. The high activity and selectivity promoted by CeO_2 have been attributed to its high capacity for metal dispersion and to its propensity to create oxygen vacancies, which promote the reduction of CO_2 into CO prior to the hydrogenation to CH_4 [59,129,133–135,197–200].

When using porous surfaces with high surface areas, the interaction between the nickel and its support is a crucial factor, determining the catalytic performance of the system with respect to its activity and selectivity for CO_2 methanation [145]. Due to the significant ability of the support to disperse the active phase, the preparation of highly dispersed metal-supported catalysts has been the focus of a variety of investigations. Reports have shown that a mesoporous nickel–alumina xerogel [72] can serve as an efficient catalyst in several reactions, due to the well-developed mesoporosity of the support and its ability to finely disperse nickel species [201]. Mesoporous nickel (35 wt %)–metal (M = Fe, Zr, Ni, Y, and Mg)

(5 wt %)–alumina xerogel catalysts with a different second metal were tested for use in CO_2 methanation. In carbon dioxide methanation reaction, the yield of CH_4 decreased in the order of 35Ni5Fe > 35Ni5Zr > 35Ni5Ni > 35Ni5Y > 35Ni5Mg. The identity of the second metal species influenced the CO_2 methanation process. The most active and selective mesoporous catalyst was 35Ni5Fe; this catalyst possesses a weak metal support interaction that is closely related to the CO dissociation energy. Fe was found to be the optimal second metal in the CO_2 methanation reaction. Fe can modify the size of metallic Ni particles and the reducibility of the Ni which leads to changes of the local electron density. These results show that the metal-support interaction, the CO dissociation energy and the pore volume influenced the CO_2 conversion. The use of a Ni/RHA–Al_2O_3 catalyst with a mesoporous structure and high surface area exhibited favorable catalytic activity [145]. Nanocrystallites of nickel oxide, such as NiO and $NiAl_2O_4$, are formed with high dispersion on the surface, suggesting a strong interaction between the metal and oxide. The catalytic activity of Ni/RHA–Al_2O_3 is better than that of Ni/SiO_2–Al_2O_3 due to its enhanced metal dispersion ability and higher chemical reaction rate. At 500 °C, a conversion of 58% and a methane selectivity of 90% were obtained [145]. On 3 w% Ni/MCM-41 catalysts, [146] a high selectivity (96.0%) were achieved at a space velocity of 5760 $kg^{-1} \cdot h^{-1}$, which was superior to the results obtained with a Ni/SiO_2 catalyst and comparable to that of a Ru/SiO_2 catalyst [106,142,202]. The high selectivity was maintained at a higher reaction temperature (400 °C). The best activity and selectivity for CO_2 methanation when using a Ni/MCM-41 mesoporous catalyst is attributed to the highly dispersed Ni^0 at 700 °C, as obtained on a surface [146]. A mesoporous catalyst of Ni/SiO_2 was reported to be more active than Ni/Al_2O_3 in CO_2 methanation [203], although other papers have reported very high activities of highly loaded Ni/Al_2O_3 catalysts [204], which even can be increased by Fe-doping [205]. Ni/ZrO_2 catalysts doped with Ce or Sm cations [196] exhibit higher catalytic activity for CO_2 methanation. This behavior can be ascribed to a synergistic effect between the surface area and doping with rare earth elements. Up to 280 °C, the Co/KIT-6 mesoporous catalyst exhibits a higher CO_2 methanation activity, with a conversion of 49% and a methane selectivity of 100% [151]. Its high methane selectivity has been attributed to the high degree of dispersion obtained on its large surface area as well as its highly ordered bicontinuous mesoporous structure.

Zeolites are an attractive support material due to their high thermal stability and large surface area. Encouraging results have been obtained for the methanation of CO [206–211] and CO_2 on zeolites [71,212]. High activity and selectivity during CO_2 methanation was reported for Y zeolite, which possesses a higher mesoporosity; in this case, the zeolite structure accounts for the improved kinetics [213]. Of the Ru/HZSM-5 and Ru/SiO_2 catalysts, the former is more selective for CH_4. This behavior can be explained by the higher amount of CO_2 that is able to react with the OH groups of the zeolite, in addition to the stronger interaction between the metal and the support. Fourier Transform Infrared (FTIR) [214] on Ru/zeolite have shown that CO_2 methanation takes place by the dissociative adsorption of CO to form CO*ad* and O*ad*, followed by conversion into CH_4 and H_2O. The hydrogenation of CO_2 has been investigated in a dielectric barrier discharge (DBD) plasma reactor packed with 10 wt % Ni/zeolite pellets within a temperature range of 180–360 °C [215]. In this case, less than 15% CO_2 conversion was observed in the catalytic system; in comparison, the non-thermal plasma created in the catalyst bed increased the conversion of CO_2 by more than 95%. These results suggest that the formation of a reactive species in the plasma reactor can speed up the rate-determining step of catalytic hydrogenation. The high conversion of CO_2 was attributed to the smaller Ni particles and their uniform dispersal over the zeolite after the plasma reaction. The hydrogenation of CO_2 involves the dissociation of CO_2 to C-O

and O on the active site of Ni/zeolite [216,217]. Ni/USY and NiCe/USY zeolite catalysts [71] exhibit high conversion rates and selectivity for methane production during CO_2 methanation. When using a large amount of Ni with a high proportion of Ni^0, the conversion is favored. The presence of CeO_2 after reduction might promote the activation of CO_2 into CO. The zeolite catalyst shows no deactivation or sintering of the Ni metal particles.

These results show that the performance of nanoporous catalyst materials depends on a variety of parameters, including particle size and shape, amount of metal, nature of the metal and the support, and evolution of the catalyst surface during thermal treatment. The role of a large pore/surface is crucial to ensure enhanced metal dispersion, high diffusivity and longer catalyst lifetime. An important aspect is the use of nanopores/nanocavities, which could favor the local increase of CO_2 concentration—nanoconfinement—and thus the consecutive conversion of intermediates with formation of CH_4.

5. Photocatalytic Reduction of CO_2 into CH_4

To replace fossil fuels with fuels derived from recycled CO_2, photovoltaics might be able to generate the energy necessary to produce these fuels. The photocatalytic reduction of CO_2 with H_2O, which is an important reaction, especially as a means of carrying out artificial photosynthesis, has been attempted in light of the importance of carbon storage [218].

The first study carried out on the photocatalytic reduction of CO_2 with H_2O used TiO_2 and $SrTiO_3$ as photocatalysts [219] and yielded HCOOH, HCHO as the principal product, and CH_3OH and CH_4 in trace amounts. Furthermore, various semiconductors, such as tungsten trioxide (WO_3), titanium dioxide (TiO_2), zinc oxide (ZnO), cadmium sulfide (CdS), gallium phosphide (GaP), and silicon carbide (SiC) activated by both xenon- and mercury-lamp irradiation, have been used for such purposes [98]. Photocatalytic CO_2 reduction is more difficult to perform and delivers with a lower efficiency [220–223] due to the associated thermodynamics and kinetics. The reduction of CO_2 by H_2O to obtain methane is a highly endothermic process (± 802 kJ·mol^{-1}) and requires a significant amount of energy. This energy is later released during the oxidation of the fuel. The reaction mechanisms for CO_2 reduction necessitate either the consecutive or simultaneous transfer of electrons and photons to the CO_2. CO_2 reduction utilizes electrons with higher reduction potential. The best-known catalysts for the photocatalytic reduction of CO_2 with water are TiO_2. It should be noted that TiO_2 is not photoresponsive under visible light irradiation, limiting its use as a photocatalyst. To obtain a photoresponse in the visible region, TiO_2 catalysts must be doped with metals [224–226], non-metals and oxygen vacancies [227,228] or noble metal doping must be used [229,230]. However, it has been observed that for reactions carried out in water, the doped photocatalysts present photoconversion but also lead to dopant metal leaching and catalyst deactivation. Excellent articles on these topics have also been published [98,218,231–240]. It has further been observed that the use of nanoparticle semiconductors can provide a higher activity for CO_2 reduction compared to the corresponding bulk semiconductor [234]. It has been observed that the photocatalytic activity increased with the decreasing diameter of the TiO_2 particles, although sunlight radiation was increasingly less utilized. However, when Pt was added to the TiO_2, a "short-circuited photoelectrochemical cell" providing both oxidizing and reducing sites for the reaction developed [234]. Often, a clear distinction between the mechanisms of the photoreduction and photoelectrochemical reduction of CO_2 is not possible, particularly when using metal-doped semiconductor materials. The reaction mechanism in the

photoreduction of CO_2 involves two important species, the hydrogen atom and carbon dioxide anion radical, which is produced by electron transfer from the conduction band.

Some investigations have pursued the development of highly dispersed transition metal oxides, such as Ti, V, Cr, Mo, inside micro- and mesoporous materials as nanophotocatalysts. Zeolites contain only isolated metal ions in their framework structures. These nanophotocatalysts can be excited under UV irradiation to form the corresponding charge-transfer excited states involved in electron transfer. The reactivities of charge-transfer excited states, *i.e.*, electron-hole pair states, are responsible for photocatalytic reactions such as the reduction of CO_2 with H_2O to produce CH_4 and CH_3OH [218,241–243]. However, in the photocatalytic reaction, CO_2 adsorbs onto the surface of the photocatalyst due to its microporosity, which permits the concentration of the substrate near reactive sites to increase and decreases the activation energy of the process. The use of microporous zeolites permits increased CO_2 adsorption and can introduce diffusion through the pores. It has also been reported that CO, CH_4, H_2, and higher hydrocarbons can be produced during the photocatalytic reduction of CO_2 on TiO_2 surfaces in the presence of gaseous H_2O [244]. In contrast, it is known that the octahedrally coordinated bulk TiO_2 photocatalyst is not selective for the photocatalytic reduction of CO_2 with gaseous H_2O. Instead, the selectivity of the photocatalytic reaction is favored on the tetrahedrally coordinated titanium dioxide photocatalysts of the silica matrix when the activity and selectivity are favored, leading to the significant formation of CH_3OH [245–249]. Ti-containing micro- and mesoporous zeolites have exhibited efficient and selective photocatalytic reactivity for the reduction of CO_2 with H_2O using UV radiation. The hydrophobicity and hydrophilicity of zeolite are additional parameters that affect the activity and selectivity of the photocatalytic reduction of CO_2 with H_2O when attempting to produce CH_4 and CH_3OH through this reaction [218]. It has been shown that the competition between CH_3OH and CH_4 is governed by the hydrophobicity/hydrophilicity of β-zeolite, as studied for the photocatalytic reduction of CO_2 with H_2O at 50 °C. The activity of hydrophilic Ti–β–OH was found to be higher than that for hydrophobic Ti–β–F. However, the selectivity for the formation of CH_3OH from Ti–β–F (41%) was higher than that from Ti–β–OH (11%). Ti–β–OH exhibited a higher reactivity compared to Ti–β–F, although its selectivity was different. On the hydrophilic Ti–β–OH zeolite, the selectivity for the formation of methane was higher than that with TS–1, Ti–β–F and P25. The selectivity for methane followed the order Ti–β–OH > TS–1 > Ti–β–F > P25. The higher activity of Ti–β–OH toward methane formation has been explained by the higher concentration of charge-transfer excited complexes. Furthermore, it has been shown previously [245,246] that the competitive interaction of CO_2 and H_2O molecules with the charge-transfer excited state of the tetrahedral titanium oxide species results in the formation of C radicals, H atoms, and OH radicals on the surface, while CH_4 and CH_3OH are formed by the reaction of C radicals with H atoms and OH radicals [245,246]. When using hydrophilic Ti–β–OH, the concentration of H_2O is significantly higher than that obtained with hydrophobic Ti–β–F, leading to a higher selectivity for the formation of methane. A higher selectivity for methane was also observed on Ti/FSM–16 [218], while the use of fluorinated Ti/FSM–16 led to the higher formation of CH_3–OH, even though the formation of methane was a major reaction pathway in both cases.

A Ti/Y zeolite containing tetrahedral isolated sites was tested for the photocatalytic reduction of CO_2 in the presence of water using UV light from a high-pressure Hg lamp (>280 nm) at 55 °C [246,247]. The tetrahedrally arranged Ti sites formed methanol with methane as the major product, while the Pt/Ti–Y zeolite selectively formed methane. In this case, CO was an apparent intermediate for the reduction of

CO_2, although H_2 was not. It is possible that the water was oxidized to OH and H^+ and that the Pt sites likely worked to suppress charge recombination [246]. Similarly, Ti–MCM–48 produced both methane and methanol, although Pt/Ti–MCM–48 was found to be the most active catalyst and selectively formed methane [247]. Ti–SBA–15 also produced methane and methanol, where methane was the major product [248–250]. The methane yield of highly dispersed tetrahedral isolated sites of titanium nanophotocatalyst was increased 300 times as compared to crystalline TiO_2. The activity was attributed to photo-excited Ti centers generated by a Ligand to Metal Charge Transfer transition ($Ti^{+IV} - O^{-II} \rightarrow Ti^{+III} - O^{-I}$) upon light absorption [248]. Pt-loading on the Ti-containing zeolite catalyst leads to an efficient quenching of the photoluminescence, accompanied by the shortening of its lifetime [235]. The reaction mechanism in the photocatalytic reduction of CO_2 with H_2O on the highly dispersed Ti oxide catalyst can be proposed to occur as follows: CO_2 and H_2O molecules interact with the excited state of the photo-induced $(Ti^{3+} - O^-)$ species, and the reduction of CO_2 and the decomposition of H_2O proceeds competitively. Furthermore, H atoms and OH• radicals are formed from H_2O and these radicals react with the carbon species formed from CO_2 to produce CH_4 and CH_3OH [235]. The reaction mechanism in the photoreduction of CO_2 involves two important species, the carbon dioxide anion radical ($CO_2 + e^- \rightarrow CO_2$) and hydrogen atom ($H^+ + e^- \rightarrow H$), which is produced by electron transfer from the conduction band. Multielectron reactions compete with these reactions (Figure 3). As observed from Figure 3, the thermodynamic potential of CO_2 reduction decreases even if several electrons and protons could be simultaneously transferred in pairs to CO_2. It is kinetically unfeasible for the reactions where all protons and electrons needed to form CH_4 and H_2O are transferred in a single step. This suggests that the appropriate photocatalyst should have photocatalytic centers in which sites transferring electrons are close enough to other sites acting as acids and transferring at least one proton according to Figure 3.

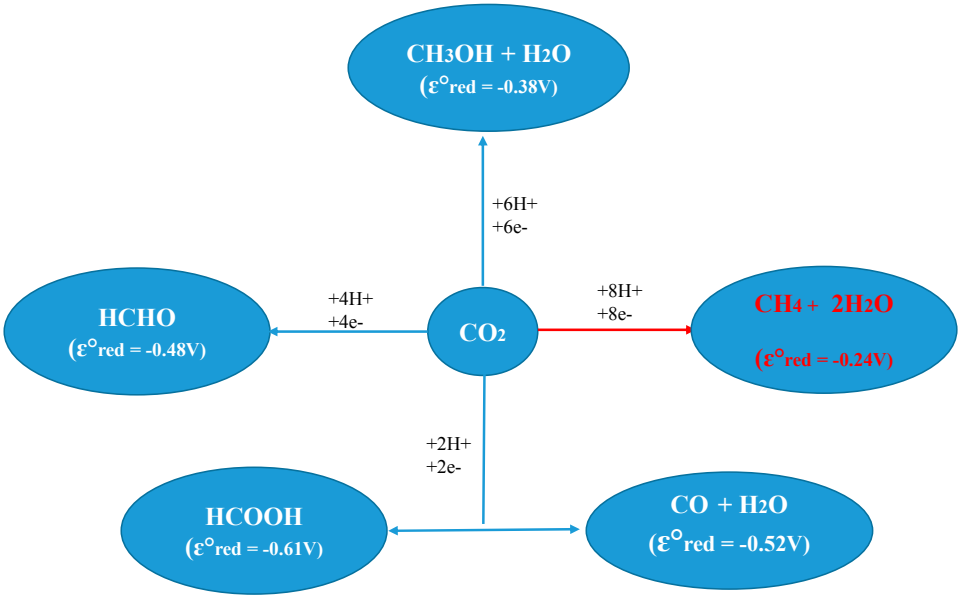

Figure 3. Photocatalytic reduction of CO_2 to fuels [98,220,221,232].

In this case an efficient photocatalyst should have appropriate catalytic sites where chemical redox processes leading to the desired products could take place with low activation barriers. The basic sites and porosity can play a favorable role in the photocatalytic process by increasing the concentration of

the substrate near the reactive sites and by decreasing the activation energy of the process. It must be noted that the solubility of CO_2 in water is low, and the CO_2 photoreduction reaction competes with H_2O_2 and H_2 formation, as follows:

$$2H_2O + 4h^+ \rightarrow O_2 + 4H^+ \quad (27)$$

$$4H^+ + 4e^- \rightarrow 2H_2 \quad (28)$$

$$O_2 + 2H^+ + 2\ e^- \rightarrow H_2O_2 \quad (29)$$

Methanol and formaldehyde are the easier products of CO_2 reduction in water solution. If the water is replaced by the other reductants such as low-polarity solvents or low-dielectric constant solvents, CO is formed as the major product. CO_2 anion radicals are strongly adsorbed on the surface through the carbon atom of another CO_2 anion radical because these radicals are not well dissolved in low-polarity solvents [98]. When a high-dielectric constant solvent is used, formic acid is formed as a major product, because the CO_2 anion radicals can be greatly stabilized by the solvent, resulting in weak interactions with the photocatalyst surface and the carbon atom of the radical reacts with a proton to produce formic acid. In order to the increase water solubility, basic pH values are necessary, but this converts CO_2 into CO_3^{2-} or HCO_3^- that are more stable and more difficult to reduce than CO_2 itself. Consequently, it could be of interest to study other solvents or to perform CO_2 reduction in the gas phase [98].

6. Conclusions

This review summarizes recent studies performed on the methanation of CO_2 on nanoporous materials. Although our knowledge of nanoporous materials is relatively well developed, several challenges remain with respect to their use in methanation processes. This review has presented an extensive series of investigations of CO_2 methanation over various catalysts. The best results concerning the activity/selectivity and the lifetime of catalysts have been obtained for Ru and Rh. However, the high costs associated with these catalysts impedes their use at large scale, such as commercial applications. Ni is the best alternative candidate due to its high selectivity for methane production. The role of the support dominates the catalyst design in terms of developing an efficient methanation catalyst, specifically with respect to ensuring enhanced metal dispersion and a long catalyst lifetime. For this reason, nanoporous materials provide the best supports for Ni (Ru, Rh, Co, Fe) particles because they can prevent sintering and deactivation through coking, which otherwise blocks the metal surface as carbon accumulates. Because the methanation reaction is extremely exothermic, the excessive heat of reaction induces metal sintering, which lowers the overall metal surface area and leads to the poor activity observed for the classical supports. Thus, it is necessary that we develop an efficient, low-temperature methanation catalyst with high thermal stability and coke formation resistance.

Many investigations have focused on CO_2 methanation, but significant effort must still be made in the coming years to understand the fundamental reaction mechanisms in order to improve the activity and the selectivity of catalysts for methane. The results of our study have demonstrated that there remains a lack of a conceptual framework regarding nanoporous catalysts and that we must enhance our understanding of the nanoarchitecture of the active sites to improve the catalytic and photocatalytic selectivity of nanomaterials toward methane. Furthermore, the results show that the use of highly dispersed small particles on supports with high surface areas and highly dispersed tetrahedrally coordinated sites

serve as the active sites for high methane selectivity. The use of nanoporous catalysts is one of the most promising approaches in the design of efficient local structures for catalysts at the molecular level, toward the development of effective methanation catalysts.

Acknowledgments

Financial support by the CNRS France is gratefully acknowledged by Ioana Fechete.

Conflicts of Interest

The authors declare no conflict of interest.

References

1. Fechete, I.; Wang, Y.; Védrine, J.C. The past, present and future of heterogeneous catalysis. *Catal. Today* **2012**, *189*, 2–27.
2. Aresta, M.; Dibenedetto, A.; Angelini, A. Catalysis for the valorization of exhaust carbon: From CO_2 to chemicals, materials, and fuels. Technological use of CO_2. *Chem. Rev.* **2014**, *114*, 1709–1742.
3. Xiaoding, X.; Moulijn, J.A. Mitigation of CO_2 by chemical conversion: Plausible chemical reactions and promising products. *Energy Fuels* **1996**, *10*, 305–325.
4. Centi, G.; Quadrelli, E.A.; Perathoner, S. Catalysis for CO_2 conversion: A key technology for rapid introduction of renewable energy in the value chain of chemical industries. *Energy Environ. Sci.* **2013**, *6*, 1711–1731.
5. Su, D.S.; Centi, G.A. Perspective on carbon materials for future energy application. *J. Energy Chem.* **2013**, *22*, 151–173.
6. Normile, D. Carbon Capture and Sequestration. *Science* **2009**, *325*, 1642–1650.
7. Shen, J.; Yin, X.; Karpuzov, D.; Semagina, N. PVP-stabilized mono- and bimetallic Ru for selective ring opening. *Catal. Sci. Technol.* **2013**, *3*, 208–221.
8. Piccolo, L.; Nassreddine, S.; Toussaint, G.; Geantet, C. Mechanism of tetralin ring opening and contraction over bifunctional Ir/SiO_2–Al_2O_3 catalysts. *ChemSusChem* **2012**, *5*, 1717–1723.
9. Fechete, I.; Ersen, O.; Garin, F.; Lazar, L.; Rach, A. Catalytic behavior of MnMCM-48 and WMnMCM-48 ordered mesoporous catalysts in a reductive environment: A study of the conversion of methylcyclopentane. *Catal. Sci. Technol*. **2013**, *3*, 444–453.
10. Vicerich, M.A.; Benitez, V.M.; Especel, C.; Epron, F.; Pieck, C.L. Influence of iridium content on the behavior of Pt-Ir/Al_2O_3 and Pt-Ir/TiO_2 catalysts for selective ring opening of naphthenes. *Appl. Catal. A* **2013**, *453*, 167–174.
11. Wang, W.; Wang, S.P.; Ma, X.B.; Gong, J.L. Recent advances in catalytic hydrogenation of carbon dioxide. *Chem. Soc. Rev.* **2011**, *40*, 3703–3727.
12. Hu, B.; Guild, C.; Suib, S.L. Thermal, electrochemical, and photochemical conversion of CO_2 to fuels and value-added products. *J. CO_2 Util.* **2013**, *1*, 18–27.
13. Samoila, P.; Epron, F.; Marecot, P.; Especel, C. Influence of chlorine on the catalytic properties of supported rhodium, iridium and platinum in ring opening of naphthenes. *Appl. Catal. A* **2013**, *462–463*, 207–219.

14. D'Ippolito, S.A.; Gutierrez, L.B.; Vera, C.R.; Pieck, C.L. Pt-Mg-Ir/Al_2O_3 and Pt-Ir/HY zeolite catalysts for SRO of decalin. Influence of Ir content and support acidity. *Appl. Catal. A* **2013**, *452*, 48–56.
15. Fechete, I.; Donnio, B.; Ersen, O.; Dintzer, T.; Djeddi, A.; Garin, F. Single crystals of mesoporous tungstenosilicate WMCM-48 molecular sieves for the conversion of methylcyclopentane (MCP) *Appl. Surf. Sci*. **2011**, *257*, 2791–2800.
16. Klein, J.; Wu, D.; Tschamber, V.; Fechete, I.; Garin, F. Carbon-NSR catalyst interaction: Impact on catalyst structure and NO_x storage efficiency. *Appl. Catal. B* **2013**, *132–133*, 527–534.
17. Omae, I. Aspects of carbon dioxide utilization. *Catal. Today* **2006**, *115*, 33–52.
18. Urda, A.; Popescu, I.; Marcu, I.C.; Carja, G.; Apostolescu, N.; Sandulescu, I. Methane and propane total oxidation on catalysts from FeLDH precursors. *Rev. Roum. Chim*. **2010**, *61*, 267–271.
19. Haddoum, S.; Fechete, I.; Donnio, B.; Garin, F.; Lutic, D.; Chitour, C.E. FeTUD-1 for the preferential rupture of the substituted C-C bond of methylcyclopentane (MCP). *Catal. Commun.* **2012**, *27*, 141–147.
20. Garbarino, G.; Riani, P.; Magistri, L.; Busca, G. A study of the methanation of carbon dioxide on Ni/Al_2O_3 catalysts at atmospheric pressure. *Int. J. Hydrog. Energy* **2014**, *39*, 11557–11565.
21. Olajire, A.A. Valorization of greenhouse carbon dioxide emissions into value-added products by catalytic processes. *J. CO_2 Util.* **2013**, *3–4*, 74–92.
22. Fechete, I.; Jouikov, V. Double decarbonylation of phthalimide revisited: A facile cathodic synthesis of isoindoline. *Electrochim. Acta* **2008**, *53*, 7107–7110.
23. Djeddi, A.; Fechete, I.; Garin, F. Selective ring opening of methylcyclopentane over titania-supported monometallic (Pt,Ir) and bimetallic (Pt-Ir) catalysts. *Top. Catal.* **2012**, *55*, 700–709.
24. Aresta, M.; Dibenedetto, A.; Angelini, A. The changing paradigm in CO_2 utilization. *J. CO_2 Util.* **2013**, *3–4*, 65–73.
25. Saeidi, S.; Amin, N.A.S.; Rahimpour, M.R. Hydrogenation of CO_2 to value-added products—A review and potential future developments. *J. CO_2 Util.* **2014**, *5*, 66–81.
26. Burkhardt, M.; Busch, G. Methanation of hydrogen and carbon dioxide. *Appl. Energy* **2013**, *111*, 74–79.
27. De Castro, J.; Rivera-Tinoco, R.; Bouallou, C. Hydrogen production from natural gas: Auto-thermal reforming and CO_2 capture. *Chem. Eng. Trans.* **2010**, *21*, 163–168.
28. Gonzalez-Garza, D.; Rivera-Tinoco, R.; Bouallou, A. Comparison of ammonia monoethylamie, diethanolamine and methyldiethanolamine solvents to reduce CO_2 greenhouse gas emissions. *Chem. Eng. Trans.* **2009**, *20*, 279–284.
29. Olajire, A.A. CO_2 capture and separation technologies for end-of-pipe applications. *Energy* **2010**, *35*, 2610–2628.
30. Olajire, A.A. A review of mineral carbonation technology in sequestration of CO_2. *J. Pet. Sci. Eng.* **2013**, *109*, 364–392.
31. Bachu, S. CO_2 storage in geological media: Role, means, status and barriers to deployment. *Prog. Energy Combust. Sci.* **2008**, *34*, 254–273.
32. Van Alphen, K.; Noothout, P.M.; Hekkert, M.P.; Turkenburg, W.C. Evaluating the development of carbon capture and storage technologies in the United States. *Renew. Sustain. Energy Rev.* **2010**, *14*, 971–998.

33. Choi, S.; Drese, J.H.; Jones, C.W. Adsorbent materials for carbon dioxide capture from large anthropogenic point sources. *ChemSusChem* **2009**, *2*, 796–854.
34. Goj, A.; Sholl, D.S.; Akten, E.D.; Kohen, D.J. Atomistic simulations of CO_2 and N_2 adsorption in silica zeolites: The impact of pore size and shape. *Phys. Chem. B* **2002**, *106*, 8367–8375.
35. Jiang, J.W.; Sandler, S.I. Separation of CO_2 and N_2 by adsorption in C168 schwarzite: A combination of 245 quantum mechanics and molecular simulation study. *J. Am. Chem. Soc.* **2005**, *127*, 11989–11997.
36. Liu B.; Smit, B. Comparative molecular simulation study of CO_2/N_2 and CH_2/N_2 separation in zeolites and metal–organic frameworks. *Langmuir* **2009**, *25*, 5918–5926.
37. Sudiro, M.; Bertucco, A. Production of synthetic gasoline and diesel fuel by alternative processes using natural gas and coal: Process simulation and optimization. *Energy* **2009**, *34*, 2206–2214.
38. Kolbe, H. Ueber Synthese der Salicylsäure. *Eur. J. Org. Chem.* **1869**, *113*, 125–127.
39. Solvay, E. Manufacture of Soda by the Ammonia Process. U.S. Patent 263,981, 5 September 1882.
40. Bosch, G. Meiser W. Process of Manufacturing Urea. U.S. Patent 1,429,483, 19 September 1922.
41. Krier, C.; Hackel, M.; Hägele, C.; Urtel, H.; Querner, C.; Haas, A. Improving the methanation process. *Chem. Ing. Tech.* **2013**, *85*, 523–528.
42. Kopyscinski, J.; Schildhauer, T.J.; Biollaz, S.M.A. Production of synthetic natural gas (SNG) from coal and dry biomass—A technology review from 1950 to 2009. *Fuel* **2010**, *89*, 1763–1783.
43. Liu, Z.; Chu, B.; Zhai, X.; Jin, Y.; Cheng, Y. Total methanation of syngas to synthetic natural gas over Ni catalyst in a micro-channel reactor. *Fuel* **2012**, *95*, 599–605.
44. Gassner, M.; Marechal, F. Thermo-economic optimization of the polygeneration of synthetic natural gas (SNG), power and heat from lignocellulosic biomass by gasification and methanation, *Energy Environ. Sci.* **2012**, *5*, 5768–5789.
45. Kienberger, T.; Zuber, C.; Novosel, K.; Baumhakl, C.; Karl, J. Desulfurization and *in situ* reduction within catalytic methanation of biogenous synthesis gas. *Fuel* **2013**, *107*, 102–112.
46. Hu, D.; Gao, J.; Ping, Y.; Jia, L.; Gunawan, P.; Zhong, Z.; Xu, G.; Gu, F.; Su, F. Enhanced investigation of CO methanation over Ni/Al_2O_3 catalysts for synthetic natural gas production. *Ind. Eng. Chem. Res.* **2012**, *51*, 4875–4886.
47. Anastas, P.T.; Kirchhoff, M.M.; Williamson, T.C. Catalysis as a foundational pillar of green chemistry. *Appl. Catal. A* **2001**, *221*, 3–13.
48. Klein, J.; Fechete, I.; Bresset, V.; Garin, F.; Tschamber, V. Effect of carbon black combustion on NO_x trap catalyst performances. *Catal. Today* **2012**, *189*, 60–64.
49. Schmidt, F. New catalyst preparation technologies-observed from an industrial viewpoint. *Appl. Catal. A* **2001**, *221*, 15–21.
50. Ertl, G. Heterogeneous catalysis on atomic scale. *J. Mol. Catal. A* **2002**, *182–183*, 5–16.
51. Djeddi, A.; Fechete, I.; Garin, F. Conversion of methylcyclopentane (MCP) on Pt/MoO_2, Ir/MoO_2 and $Pt\text{-}Ir/MoO_2$ catalysts. *Catal. Commun.* **2012**, *17*, 173–178.
52. Moon, D.J. Hydrogen production by catalytic reforming of gaseous hydrocarbons (methane & LPG). *Catal. Surv. Asia* **2008**, *12*, 188–202.
53. Boulaoued, A.; Fechete, I.; Donnio, B.; Bernard, M.; Turek, P.; Garin, F. Mo/KIT-6, Fe/KIT-6 and Mo-Fe/KIT-6 as new types of heterogeneous catalysts for the conversion of MCP. *Microporous Mesoporous Mater.* **2012**, *155*, 131–142.

54. Haller, G.L. New catalytic concepts from new materials: Understanding catalysis from a fundamental perspective, past, present, and future. *J. Catal.* **2003**, *216*, 12–22.
55. Especel, C.; Duprez, D.; Epron F. Bimetallic catalysts for hydrogenation in liquid phase. *C. R. Chim.* **2014**, *17*, 790–800.
56. Ascaso, S.; Gálvez, M.E.; da Costa, P.; Moliner, R.; Lázaro, M.J. On the influence of the alumina precursor in Fe-K/Al_2O_3 structured catalysts for the simultaneous removal of soot and NO_x: From surface properties to reaction mechanism. *C. R. Chim.* **2014**, *7–8*, 681–686.
57. Budzianowski, W.M. Negative carbon intensity of renewable energy technologies involving biomass or carbon dioxide as inputs. *Renew. Sustain. Energy Rev*. **2012**, *16*, 6507–6521.
58. Budzianowski, W.M. Value-added carbon management technologies for low CO_2 intensive carbon-based energy vectors. *Energy* **2012**, *41*, 280–297.
59. Sharma, S.; Hu, Z.; Zhang, P.; McFarland, E.W.; Metiu, H. CO_2 methanation on Ru-doped ceria. *J. Catal.* **2011**, *278*, 297–309.
60. Caballero, A.; Perez, P.J. Methane as raw material in synthetic chemistry: The final frontier. *Chem. Soc. Rev.* **2013**, *42*, 8809–8820.
61. Herranz, T.; Rojas, S.; Perez-Alonso, F.J.; Ojeda, M.; Terreros, P.; Fierro, J.L.G. Hydrogenation of carbon oxides over promoted Fe–Mn catalysts prepared by the microemulsion methodology. *Appl. Catal. A* **2006**, *311*, 66–75.
62. Janke, C.; Duyar, M.S.; Hoskins, M.; Farrauto, R. Catalytic and adsorption studies of the hydrogenation of CO_2 to methane. *Appl. Catal. B* **2014**, *152–153*, 184–191.
63. Abello, S.; Berrueco, C.; Montane, D. High-loaded nickel–alumina catalyst for direct CO_2 hydrogenation into synthetic natural gas (SNG). *Fuel* **2013**, *113*, 598–609.
64. Holy, N.L.; Carey, T.F. Ethanol and *n*-propanol from syngas. *Appl. Catal*. **1985**, *19*, 219–223.
65. Shustorovich, E.; Bell, A.T. Analysis of CO hydrogenation pathways using the bond-order-conservation method. *J. Catal.* **1988**, *113*, 341–352.
66. Karelovic, A.; Ruiz, P. Mechanistic study of low temperature CO_2 methanation over Rh/TiO_2 catalysts. *J. Catal.* **2013**, *301*, 141–153.
67. Andersson, M.P.; Abild-Pedersen, F.; Remediakis, I.N.; Bligaard, T.; Jones, G.; Engbæk, J.; Lytken, O.; Horch, S.; Nielsen, J.H.; Sehested, J.; *et al.* Structure sensitivity of the methanation reaction: H_2-induced CO dissociation on nickel surfaces. *J. Catal.* **2008**, *255*, 6–19.
68. Aksoylu, A.E.; Önsan, Z.İ. Kinetics of CO Hydrogenation over Ni−Mo/Al_2O_3 catalysts with and without K promotion. *Ind. Eng. Chem. Res.* **1998**, *37*, 2397–2403.
69. Krylov, O.V.; Mamedov, A.K. Heterogeneous catalytic reactions of carbon dioxide. *Russ. Chem. Rev.* **1995**, *64*, 877–900.
70. Kowalczyk, Z.; Stołecki, K.; Pilecka, G.W.R.; Miskiewicz, E.; Wilczkowska, E.; Karpinski, Z. Supported ruthenium catalysts for selective methanation of carbon oxides at very low CO_x/H_2 ratios. *Appl. Catal. A* **2008**, *342*, 35–39.
71. Graca, I.; González, L.V.; Bacariza, M.C.; Fernandes, A.; Henriques, C.; Lopes, J.M.; Ribeiro, M.F. CO_2 hydrogenation into CH_4 on NiHNaUSY zeolites. *Appl. Catal. B* **2014**, *147*, 101–110.
72. Hwang, S.; Hong, U.G.; Lee, J.; Baik, J.H.; Koh, D.J.; Lim, H.; Song, I.K. Methanation of carbon dioxide over mesoporous nickel–M–alumina (M = Fe, Zr, Ni, Y, and Mg) xerogel catalysts: Effect of second metal. *Catal. Lett.* **2012**, *142*, 860–868.

73. Jiang, J.; Babarao, R.; Hu, Z. Molecular simulations for energy, environmental and pharmaceutical applications of nanoporous materials: From zeolites, metal–organic frameworks to protein crystals. *Chem. Soc. Rev.* **2011**, *40*, 3599–3612.
74. Fechete, I.; Caullet, P.; Dumitriu, E.; Hulea, V.; Kessler, H. Study of the conversion of aromatic hydrocarbons on EMT-type zeolite. Influence of the partial substitution of Al by Ga. *Appl. Catal. A* **2005**, *280*, 245–254.
75. Taguchi, A.; Schuth, F. Ordered mesoporous materials in catalysis. *Microporous Mesoporous Mater.* **2005**, *77*, 1–45.
76. Fabiano, D.P.; Hamad, B.; Cardoso, D.; Essayem, N. On the understanding of the remarkable activity of template-containing mesoporous molecular sieves in the transesterification of rapeseed oil with ethanol. *J. Catal.* **2010**, *276*, 190–196.
77. Rothw, W.; Cejka, J. Two-dimensional zeolites: Dream or reality? *J. Catal. Sci. Technol*. **2011**, *1*, 43–53.
78. Fechete, I.; Debbih-Boustila, S.; Merkache, R.; Hulea, O.; Lazar, L.; Lutic, D.; Balasanian, I.; Garin, F. MnMCM-48, CoMCM-48 and CoMnMCM-48 mesoporous catalysts for the conversion of methylcyclopentane (MCP). *Environ. Eng. Manag. J.* **2012**, *11*, 1931–1943.
79. Garrone, E.; Fajula, F. Acidity and basicity of ordered silica-based mesoporous materials. *Mol. Sieves* **2008**, *6*, 213–267.
80. Auroux, A. Acidity and Basicity determination by adsorption microcalorimetry. *Mol. Sieves* **2008**, *6*, 45–152.
81. Lauron-Pernot, H. Evaluation of surface acido-basic properties of inorganic-based solids by model catalytic alcohol reaction networks. *Catal. Rev.* **2006**, *48*, 315–361.
82. Fechete, I.; Simon-Masseron, A.; Dumitriu, E.; Lutic, D.; Caullet, P.; Kessler, H. The role of acidity of CeH–EMT–type zeolite for catalyzing toluene alkylation with methanol to xylenes. *Rev. Roum. Chim.* **2008**, *53*, 55–61.
83. Cejka, J.; Centi, G.; Perez-Pariente, J.; Roth, W.J. Zeolite-based materials for novel catalytic applications: Opportunities, perspectives and open problems. *Catal. Today* **2012**, *179*, 2–15.
84. Vinh-Thang, H.; Huang, Q.; Ungureanu, A.; Eić, M.; Trong-On, D.; Kaliaguine, S. Effect of the acid properties on the diffusion of C_7 hydrocarbons in UL-ZSM-5 materials. *Microporous Mesoporous Mater.* **2006**, *92*, 117–128.
85. Fechete, I.; Gautron, E.; Dumitriu, E.; Lutic, D.; Caullet, P.; Kessler, H. Studies on the acidity and the stability of Fe^{3+} ions in the framework (Si,Fe)–MCM–22 zeolite. Selective para-xylene production by toluene disproportionation. *Rev. Roum. Chim.* **2008**, *53*, 49–54.
86. Valange, S.; Derouault, A.; Barrault, J.; Gabelica, Z. One-step generation of highly selective hydrogenation catalysts involving sub-nanometric Cu_2O supported on mesoporous alumina: strategies to control their size and dispersion. *J. Mol. Catal. A* **2005**, *228*, 255–266.
87. Nair, M.; Yen, H.; Kleitz, F. Nanocast mesoporous mixed metal oxides for catalytic applications. *C. R. Chim.* **2014**, *17*, 641–655.
88. Trouvé, A.; Batonneau-Gener, I.; Valange, S.; Bonne, M.; Mignard, S. Tuning the hydrophobicity of mesoporous silica materials for the adsorption of organic pollutant in aqueous solution. *J. Hazard. Mater.* **2012**, *201–202*, 107–114.

89. Meloni, D.; Monaci, R.; Rombi, E.; Guimon, C.; Martinez, H.; Fechete, I.; Dumitriu, E. Synthesis and characterization of MCM-22 zeolite for the N_2O oxidation of benzene to phenol. *Stud. Surf. Sci. Catal. A* **2002**, *142*, 167–174.
90. Serna, P.; Gates, B.C. Zeolite- and MgO-supported rhodium complexes and rhodium clusters: Tuning catalytic properties to control carbon–carbon *vs.* carbon–hydrogen bond formation reactions of ethene in the presence of H_2. *J. Catal.* **2013**, *308*, 201–212.
91. Montes de Correa, C.; Castrillon, F.C. Supported bimetallic Pd-Co catalysts: Characterization and catalytic activity. *J. Mol. Catal. A* **2005**, *228*, 267–273.
92. Vedrine, J.C. Revisiting active sites in heterogeneous catalysis: Their structure and their dynamic behaviour. *Appl. Catal. A* **2014**, *474*, 40–50.
93. Bensacia, N.; Fechete, I.; Moulay, S.; Hulea, O.; Boos, A.; Garin, F. Kinetic and equilibrium studies of lead (II) adsorption from aqueous media by KIT-6 mesoporous silica functionalized with—COOH. *C. R. Chim.* **2014**, *17*, 869–880.
94. Derouane, E.G.; Védrine, J.C.; Ramos Pinto, R.; Borges, P.M.; Costa, L.; Lemos, M.A.N.D.A.; Lemos, F.; Ribeiro, F.R. The acidity of zeolites: Concepts, measurements and relation to catalysis: A review on experimental and theoretical methods for the study of zeolite acidity. *Catal. Rev.* **2013**, *55*, 454–515.
95. Verboekend, D.; Perez-Ramırez, J. Design of hierarchical zeolite catalysts by desilication. *Catal. Sci. Technol.* **2011**, *1*, 879–890.
96. Bensacia, N.; Fechete, I.; Moulay, S.; Boos, A.; Garin, F. Removal of cadmium (II) from aqueous media using COOH/TUD-1 mesoporous solid. Kinetic and thermodynamic studies. *Environ. Eng. Manag. J.* **2014**, *13*, 2675–2686.
97. Centi, G.; Genovese, C.; Giordano, G.; Katovic, A.; Perathoner, S. Performance of Fe-BEA catalysts for the selective hydroxylation of benzene with N_2O. *Catal. Today* **2004**, *91–92*, 17–26.
98. Centi, G.; Perathoner, S. Opportunities and prospect in the chemical recycling of carbon dioxide to fuels. *Catal. Today* **2009**, *148*, 191–205.
99. Zhang, G.; Sun, T.; Peng, J.; Wang, S.; Wang, S. A comparison of Ni/SiC and Ni/Al_2O_3 catalyzed total methanation for production of synthetic natural gas. *Appl. Catal. A* **2013**, *462–463*, 75–81.
100. Zangeneh, F.T.; Sahebdelfar, S.; Ravanchi, M.T. Conversion of carbon dioxide to valuable petrochemicals: An approach to clean development mechanism. *J. Nat. Gas Chem.* **2011**, *20*, 219–231.
101. Behn, A. The synthesis of organic chemicals by catalytic reactions of carbon dioxide. *Bull. Soc. Chim. Belg.* **1985**, *94*, 671–683.
102. Inoue, S.; Yamazaki, Y. *Organic and Bio-Organic Chemistry of Carbon Dioxide*; Inoue, S., Yamazaki, Y., Eds.; Kodansha: Tokyo, Japan, 1982.
103. Ma, J.; Sun, N.; Zhang, X.; Zhao, N.; Xiao, F.; Wei, W.; Sun, Y. A short review of catalysis for CO_2 conversion. *Catal. Today* **2009**, *148*, 221–231.
104. Falconer, J.L.; Zagli, A.E. Adsorption and methanation of carbon dioxide on a nickel/silica catalyst. *J. Catal.* **1980**, *62*, 280–285.
105. Weatherbee, G.D.; Bartholomew, C.H. Hydrogenation of CO_2 on group VIII metals: II. Kinetics and mechanism of CO_2 hydrogenation on nickel. *J. Catal.* **1982**, *77*, 460–472.

106. Peebles, D.E.; Goodman, D.W.; White, J.M. Methanation of carbon dioxide on nickel (100) and the effects of surface modifiers. *J. Phys. Chem.* **1983**, *87*, 4378–4387.
107. Marwood, M.; Doepper, R.; Renken, A. *In-situ* surface and gas phase analysis for kinetic studies under transient conditions. The catalytic hydrogenation of CO_2. *Appl. Catal. A* **1997**, *151*, 223–246.
108. Lapidus, A.L.; Gaidai, N.A.; Nekrasov, N.V.; Tishkova, L.A.; Agafonov, Y.A.; Myshenkova, T.N. The mechanism of carbon dioxide hydrogenation on copper and nickel catalysts. *Pet. Chem.* **2007**, *47*, 75–82.
109. Fujita, S.; Terunuma, H.; Kobayashi H.; Takezawa, N. Methanation of carbon monoxide and carbon dioxide over nickel catalyst under the transient state. *React. Kinet. Catal. Lett.* **1987**, *33*, 179–184.
110. Schild, C.; Wokaun, A.; Baiker, A. On the mechanism of CO and CO_2 hydrogenation reactions on zirconia-supported catalysts: A diffuse reflectance FTIR study: Part II. Surface species on copper/zirconia catalysts: Implications for methanoi synthesis selectivity. *J. Mol. Catal.* **1990**, *63*, 243–254.
111. Emmett, P.H. *Catalysis*; Emmett, P.H., Ed.; Reinhold: New York, NY, USA, 1951; Volume 4, pp. 299–303.
112. Oki, S.; Mezaki, R. Identification of rate-controlling steps for the water-gas shift reaction over an iron oxide catalyst. *J. Phys. Chem.* **1973**, *77*, 447–452.
113. Oki, S.; Mezaki, R. Mechanistic structure of the water-gas shift reaction in the vicinity of chemical equilibrium. *J. Phys. Chem.* **1973**, *77*, 1601–1605.
114. Lunde, P.J.; Kester, F.L. Rates of methane formation from carbon dioxide and hydrogen over a ruthenium catalyst. *J. Catal.* **1973**, *30*, 423–429.
115. Doehlemann, E. The mechanism of the water-gas reaction on an iron catalyst. *Z. Elektrochem*. **1938**, *44*, 178–183.
116. Kulkova, N.V.; Temkin, M.I. Kinetics of the reaction of conversion of carbon monoxide by water vapor. *Zh. Fiz. Khim.* **1949**, *23*, 695–713.
117. Kul'kova, N.V.; Kuznets, Z.D.; Temkin, M.I. The exchange of oxygen isotopes between carbon monoxide and carbon dioxide on an iron oxide catalyst. *Dokl. Akad. Nauk SSSR* **1953**, *90*, 1067–1070.
118. Wagner, C. *Adsorbed Atomic Species as Intermediates in Heterogeneous Catalysisis*; Eley, D.D., Ed.; Academic Press: New York, NY, USA, 1970; Volume 21, pp. 323–381.
119. Jacquemin, M.; Beuls, A.; Ruiz, P. Catalytic production of methane from CO_2 and H_2 at low temperature: Insight on the reaction mechanism. *Catal. Today* **2010**, *157*, 462–466.
120. Watwe, R.M.; Bengaard, H.S.; Rostrup-Nielsen, J.R.; Dumesic, J.A.; Norskov, J.K. Theoretical studies of stability and reactivity of CH_x species on Ni(111). *J. Catal.* **2000**, *189*, 16–30.
121. Ackermann, M.; Robach, O.; Walker, C.; Quiros, C.; Isern H.; Ferrer, S. Hydrogenation of carbon monoxide on Ni(III) investigated with surface X-ray diffraction at atmospheric pressure. *Surf. Sci.* **2004**, *557*, 21–30.
122. Fujita, S.I.; Nakamura, M.; Doi, T.; Takezawa, N. Mechanisms of methanation of carbon dioxide and carbon monoxide over nickel/alumina catalysts. *Appl. Catal. A* **1993**, *104*, 87–100.

123. Choe, S.J.; Kang, H.J.; Kim, S.J.; Park, S.B.; Park, D.H.; Huh, D.S. Adsorbed carbon formation and carbon hydrogenation for CO_2 methanation on the Ni(111) surface: ASED-MO study. *Bull. Korean Chem. Soc.* **2005**, *26*, 1682–1688.
124. Solymosi, F.; Erdohelyi, A.; Bansagi, T. Methanation of CO_2 on supported rhodium catalyst. *J. Catal.* **1981**, *68*, 371–382.
125. Ibraeva, Z.A.; Nekrasov, N.V.; Gudkov, B.S.; Yakerson, V.I.; Beisembaeva, Z.T.; Golosman, E.Z.; Kiperman, S.L. Kinetics of methanation of carbon dioxide on a nickel catalyst. *Theor. Exp. Chem.* **1990**, *26*, 620–624.
126. Kim, H.Y.; Lee, H.M.; Park, J.N. Bifunctional mechanism of CO_2 methanation on Pd-MgO/SiO_2 catalyst: Independent roles of MgO and Pd on CO_2 methanation. *J. Phys. Chem. C* **2010**, *114*, 7128–7131.
127. Sehested, J.; Dahl, S.; Jacobsen, J.; Rostrup-Nielsen, J.R. Methanation of CO over nickel: mechanism and kinetics at high H_2/CO ratios. *J. Phys. Chem. B* **2005**, *109*, 2432–2438.
128. Fisher, I.A.; Bell, A.T. A Comparative study of CO and CO_2 hydrogenation over Rh/SiO_2. *J. Catal.* **1996**, *162*, 54–65.
129. De Leitenburg, C.; Trovarelli, A.; Kaspar, J. A temperature-programmed and transient kinetic study of CO_2 activation and methanation over CeO_2 supported noble metals. *J. Catal.* **1997**, *166*, 98–107.
130. Beuls, A.; Swalus, C.; Jacquemin, M.; Heyen, G.; Karelovic, A.; Ruiz, P. Methanation of CO_2: Further insight into the mechanism over Rh/γ-Al_2O_3 catalyst. *Appl. Catal. B* **2012**, *113–114*, 2–10.
131. Park, J.N.; McFarland, E.W. A highly dispersed Pd–Mg/SiO_2 catalyst active for methanation of CO_2. *J. Catal.* **2009**, *266*, 92–97.
132. Sanchez-Escribano, V.; Larrubia-Vargas, M.A.; Busca, G. On the mechanisms and the selectivity determining steps in syngas conversion over supported metal catalysts: An IR study. *Appl. Catal. A* **2007**, *316*, 68–74.
133. Trovarelli, A.; de Leitenburg, C.; Dolcetti, G. CO and CO_2 hydrogenation under transient conditions over Rh–CeO_2: Novel positive effects of metal-support interaction on catalytic activity and selectivity. *J. Chem. Soc. Chem. Commun.* **1991**, 472–473, doi:10.1039/C39910000472.
134. Trovarelli, A.; de Leitenburg, C.; Dolcetti, G.; Llorca, J. CO_2 methanation under transient and steady-state conditions over Rh/CeO_2 and CeO_2-promoted Rh/SiO_2: The role of surface and bulk ceria. *J. Catal.* **1995**, *151*, 111–124.
135. Tada, S.; Shimizu, T.; Kameyama, H.; Haneda, T.; Kikuchi, R. Ni/CeO_2 catalysts with high CO_2 methanation activity and high CH_4 selectivity at low temperatures. *Int. J. Hydrog. Energy* **2012**, *37*, 5527–5531.
136. Park, H.-A.; Choi, J.H.; Choi, K.M.; Lee, D.K.; Kang, J.K. Highly porous gallium oxide with a high CO_2 affinity for the photocatalytic conversion of carbon dioxide into methane. *J. Mater. Chem.* **2012**, *22*, 5304–5307.
137. Sabatier, P.; Senderens, J.B. New Synthesis of Methane. C. R. *Acad. Sci. Paris* **1902**, *134*, 514–516.
138. Inui, T.; Takeguchi, T. Effective conversion of carbon dioxide and hydrogen to hydrocarbons. *Catal. Today* **1991**, *10*, 95–106.
139. Wang, W.; Gong, J. Methanation of carbon dioxide: An Overview. *Front. Chem. Eng. China* **2011**, *5*, 2–10.

140. Fujita, S.I.; Takezawa, N. Difference in the selectivity of CO and CO_2. Methanation reactions. *Chem. Eng. J.* **1997**, *68*, 63–68.
141. Aksoylu, A.E.; Misirli, Z.; Onsan, I. Interaction between nickel and molybdenum in Ni–Mo/Al_2O_3 catalysts: I: CO_2 methanation and SEM-TEM studies. *Appl. Catal. A* **1998**, *168*, 385–397.
142. Weatherbee, G.D.; Bartholomew, C.H. Hydrogenation of CO_2 on group VIII metals: I. Specific activity of Ni/SiO_2. *J. Catal.* **1981**, *68*, 67–76.
143. Yamasaki, M.; Habazaki, H.; Asami, K.; Izumiya, K.; Hashimoto, K. Effect of tetragonal ZrO_2 on the catalytic activity of Ni/ZrO_2 catalyst prepared from amorphous Ni–Zr alloys. *Catal. Commun.* **2006**, *7*, 24–28.
144. Yamasaki, M.; Komori, M.; Akiyama, E.; Habazaki, H.; Kawashima, A.; Asami, K.; Hashimoto, K. CO_2 methanation catalysts prepared from amorphous Ni–Zr–Sm and Ni–Zr–misch metal alloy precursors. *Mater. Sci. Eng. A* **1999**, *267*, 220–226.
145. Chang, F.W.; Kuo, M.S.; Tsay, M.T.; Hsieh, M.C. Hydrogenation of CO_2 over nickel catalysts on rice husk ash-alumina prepared by incipient wetness impregnation. *Appl. Catal. A* **2003**, *247*, 309–320.
146. Du, G.; Lim, S.; Yang, Y.; Wang, C.; Pfefferle, L.; Haller, G.L. Methanation of carbon dioxide on Ni-incorporated MCM-41 catalysts: The influence of catalyst pretreatment and study of steady-state reaction. *J. Catal.* **2007**, *249*, 370–379.
147. Yasuda, H.; Choi, J.-C.; Lee, S.-C.; Sakakura, T. Reactivity of diaryloxy palladium complex with TMEDA (*N*,*N*,*N*',*N*'-Tetramethylethylenediamine) ligand toward carbon monoxide and carbon dioxide. *Organometallics* **2002**, *21*, 1216–1220.
148. Vol'pin, M.E.; Kolomnikov, I.S. Reactions of carbon dioxide with transition metal compounds. *Pure Appl. Chem.* **1973**, *33*, 567–582.
149. Lee, D.; Harper, A.S.; DeSimone, J.M.; Murray, R.W. Ion atmosphere relaxation control of electron transfer dynamics in a plasticized carbon dioxide redox polyether melt. *J. Am. Chem. Soc.* **2003**, *125*, 1096–1103.
150. Bergquist, C.; Fillebeen, T.; Morlok, M.M.; Parkin, G. Protonation and reactivity towards carbon dioxide of the mononuclear tetrahedral zinc and cobalt hydroxide complexes, [TpBut,Me]ZnOH and [TpBut,Me]CoOH: Comparison of the reactivity of the metal hydroxide function in synthetic analogues of carbonic anhydrase. *J. Am. Chem. Soc.* **2003**, *125*, 6189–6199.
151. Zhou, G.; Wu, T.; Xie, H.M.; Zheng, X.X. Effects of structure on the carbon dioxide methanation performance of Co-based catalysts. *Int. J. Hydrog. Energy* **2013**, *38*, 10012–10018.
152. Choi, J.-C.; Sakakura, T. Roles played in the photocatalytic activation of hydrocarbons. *J. Am. Chem. Soc.* **2003**, *125*, 7762–7763.
153. Dahlenburg, L.; Prengel, C. Alkyl and aryl compounds of iridium and rhodium. 18. Oligophosphine ligands. 6. Reactivity of some alkyls and aryls of rhodium and iridium toward carbon dioxide. Facile formation and x-ray structural characterization of the peroxocarbonato complex [cyclic]—mer—Rh (4-MeC_6H_4) [OOC(O)O][PhP($CH_2CH_2CH_2PPh_2$)$_2$]. *Organometallics* **1984**, *3*, 934–936.
154. Tetrick, S.M.; Xu, C.; Pinkes, J.R.; Cutler, A.R. Synthesis of M_2Rh_2 Bis (μ3-carbon dioxide) complexes from the reaction between [Rh(OH)(η4-COD)]$_2$ and cationic metal carbonyls. *Organometallics* **1998**, *17*, 1861–1867.

155. Tang, Y.; Zakharov, L.N.; Rheingold, A.L.; Kemp, R.A. Insertion of carbon dioxide into Mg-N bonds. Structural characterization of a previously unknown η2 chelation mode to magnesium in magnesium carbamates. *Organometallics* **2004**, *23*, 4788–4791.
156. Loferer, M.J.; Tautermann, C.S.; Loeffler, H.H.; Liedl, K.R. Influence of backbone conformations of human carbonic anhydrase II on carbon dioxide hydration: Hydration pathways and binding of bicarbonate. *J. Am. Chem. Soc.* **2003**, *125*, 8921–8927.
157. Yasuda, H.; Okamoto, T.; Matsuoka, Y.; Nakamura, A.; Kai, Y.; Kanehisa, N.; Kasai, N. Diverse reaction courses in the controlled carbometalation of heterocumulenes with zirconium-diene complexes and molecular structures of carbon dioxide, isocyanate and ketene 1:1 and 1:2 inserted compounds. *Organometallics* **1989**, *8*, 1139–1152.
158. Pinkes, J.R.; Steffey, B.D.; Vites, J.C.; Cutler, A.R. Carbon dioxide insertion into the iron-zirconium and ruthenium-zirconium bonds of the heterobimetallic complexes $Cp(CO)_2MZr(Cl)Cp_2$: Direct production of the .mu.-.eta.1(C): Eta.2(*O*,*O*')-CO_2 compounds $Cp(CO)_2MCO_2Zr(Cl)Cp_2$. *Organometallics* **1994**, *13*, 21–23.
159. Klingler, R.J.; Bloom, I.; Rathke, J.W. Thermodynamics for the addition of a tin hydride to carbon dioxide. *Organometallics* **1985**, *4*, 1893–1894.
160. Lescop, C.; Arliguie, T.; Lance, M.; Nierlich, M.; Ephritikhine, M. Bis pentamethyl cyclopentadienyl uranium (IV) thiolate compounds. Synthesis and reactions with CO_2 and CS_2. *J. Organomet. Chem.* **1999**, *580*, 137–144.
161. Blake, R.E., Jr.; Antonelli, D.M.; Henling, L.M.; Schaefer, W.P.; Hardcastle, K.I.; Bercaw, J.E. A cationic imido complex of permethyltantalocene: H_2 and carbon-hydrogen bond activation, [2+2] cycloaddition reactions, and an unusual reaction with carbon dioxide that affords coordinated isocyanate. *Organometallics* **1998**, *17*, 718–725.
162. Antinolo, A.; Carrillo-Hermosilla, F.; del Hierro, I.; Otero, A.; Fajardo, M.; Mugnier, Y. Synthesis and characterization of new alkyl-carbon dioxide compounds and the first neutral acyl-carbonyl niobocene complexes. *Organometallics* **1997**, *16*, 4161–4166.
163. Souter, P.F.; Andrews, L. A spectroscopic and theoretical study of the reactions of group 6 metal atoms with carbon dioxide. *J. Am. Chem. Soc.* **1997**, *119*, 7350–7360.
164. Chetcuti, P.A.; Knobler, C.B.; Hawthorne, M.F. Intramolecular conversion of a five-membered iridacycle to a three-membered counterpart by carbon dioxide extrusion. *Organometallics* **1986**, *5*, 1913–1914.
165. Vivanco, M.; Ruiz, J.; Floriani, C.; Chiesi-Villa, A.; Guastini, C. Stepwise insertion of isocyanides and carbon dioxide into vanadium-aryl bonds: Chemistry of a tris (eta.2-iminoacyl) vanadium(III) complex. *Organometallics* **1990**, *9*, 2185–2187.
166. Tsuda, T.; Ueda, K.; Saegusa, T. Carbon dioxide insertion into organocopper and organosilver compounds. *J. Chem. Soc. Chem. Comm.* **1974**, 380–381, doi:10.1039/C39740000380.
167. Vivanco, M.; Ruiz, J.; Floriani, C.; Chiesi-Villa, A.; Rizzoli, C. Chemistry of the vanadium-carbon sigma. bond. 1. Insertion of carbon monoxide, isocyanides, carbon dioxide, and heterocumulenes into the V-C bond of tris(mesityl)vanadium(III). *Organometallics* **1993**, *12*, 1794–1801.
168. Galindo, A.; Pastor, A.; Perez, P.J.; Carmona, E. Bis (ethylene) complexes of molybdenum and tungsten and their reactivity toward carbon dioxide. New examples of acrylate formation by coupling of ethylene and carbon dioxide. *Organometallics* **1993**, *12*, 4443–4451.

169. Darensbourg, D.J.; Kudaroski, R.; Delord, T. Synthesis and X-ray structure of anionic chelating phosphine-acyl derivative of tungsten, [cyclic] [PPh_4][$W(CO)_4C(O)CH_2CH_2CH_2PPh_2$], and the reactivity of its decarbonylated analog with carbon dioxide. *Organometallics* **1985**, *4*, 1094–1097.
170. Birdwhistell, K.R.; Templeton, J.L. Reactions at the β-carbon of anionic tungsten acetylide complexes: Ion pairing, vinylidene formation, and carbon dioxide binding. *Organometallics* **1985**, *4*, 2062–2064.
171. Carmona, E.; Munoz, M.A.; Perez, P.J.; Poveda, M.L. Rotational isomerism in bis (carbon dioxide) complexes of molybdenum generated by conrotatory motion of the CO_2 ligands. *Organometallics* **1990**, *9*, 1337–1339.
172. Alvarez, R.; Carmona, E.; Galindo, A.; Gutierrez, E.; Marın, J.M.; Monge, A.; Poveda, M.L.; Ruiz, C.; Savariault, J.M. Formation of carboxylate complexes from the reactions of carbon dioxide with ethylene complexes of molybdenum and tungsten. X-ray and neutron diffraction studies. *Organometallics* **1989**, *8*, 2430–2439.
173. Fong, L.K.; Fox, J.R.; Cooper, N.J. Reactions of carbon dioxide with the electron-rich polyhydride complex [$Mo(dmpe)_2H_4$]. *Organometallics* **1987**, *6*, 223–231.
174. Mandal, S.K.; Ho, D.M.; Orchin, M. Reaction of electrophiles with manganese(I) and rhenium(I) alkoxide complexes: Reversible absorption of atmospheric carbon dioxide. *Organometallics* **1993**, *12*, 1714–1719.
175. Darensbourg, D.J.; Lee, W.-Z.; Phelps, A.L.; Guidry, E. Kinetic study of the insertion and deinsertion of carbon dioxide into fac-$(CO)_3$(dppe)MnOR derivatives. *Organometallics* **2003**, *22*, 5585–5588.
176. Johnston, R.F.; Cooper, J.C. The first example of photochemically activated carbon dioxide insertion into transition-metal-carbon bonds. *Organometallics* **1987**, *6*, 2448–2449.
177. Kirchbauer, F.G.; Pellny, P.-M.; Sun, H.; Burlakov, V.V.; Arndt, P.; Baumann, W.; Spannenberg, A.; Rosenthal, U. Synthesis and reactions with carbon dioxide of mono (σ-alkynyl) Titanocene (III) Complexes Cp*2Ti(C□CR) (R = Me, *t*-Bu) and the Corresponding "Ate" Complexes [Cp*2Ti(C□CR)$_2$Li(THF)$_n$] (R = SiMe3, *t*-Bu, Ph). *Organometallics* **2001**, *20*, 5289–5296.
178. Giuseppetti, M.E.; Cutler, A.R. Metallocarboxylate trialkylsilyl esters: A means of derivatizing the carbon dioxide-containing [.eta.1-C] metallocarboxylates $Cp(CO)_2FeCO_2$-Li^+ and $Cp(CO)_2FeCO_2$-Na^+. *Organometallics* **1987**, *6*, 970–973.
179. Hirano, M.; Akita, M.; Tani, K.; Kumagai, K.; Kasuga, N.C.; Fukuoka, A.; Komiya, S. Activation of coordinated carbon dioxide in $Fe(CO_2)(depe)_2$ by group 14 electrophiles. *Organometallics* **1997**, *16*, 4206–4213.
180. Choi, P.H.; Jun, K.-W.; Lee, S.-J.; Choi, M.-J.; Lee, K.-W. Hydrogenation of carbon dioxide over alumina supported Fe-K catalysts. *Catal. Lett.* **1996**, *40*, 115–118.
181. Satthawong, R.; Koizumi, N.; Song, C.; Prasassarakich, P. Comparative study on CO_2 hydrogenation to higher hydrocarbons over Fe-Based bimetallic catalysts. *Top. Catal.* **2014**, *57*, 588–594.
182. Chang, F.-W.; Hsiao, T.-J.; Shih, J.-D. Hydrogenation of CO_2 over a rice husk ash supported nickel catalyst prepared by deposition-precipitation. *Ind. Eng. Chem. Res.* **1998**, *37*, 3838–3845.
183. Zagli, E.; Falconer, J. Carbon dioxide adsorption and methanation on ruthenium. *J. Catal.* **1981**, *69*, 1–8.

184. Panagiotopoulou, P.; Kondarides, D.I.; Verykios, X.E. Selective methanation of CO over supported noble metal catalysts: Effects of the nature of the metallic phase on catalytic performance. *Appl. Catal. A* **2008**, *344*, 45–54.
185. Weatherbee, G.D.; Bartholomew, C.H. Hydrogenation of CO_2 on group VIII metals: IV. Specific activities and selectivities of silica-supported Co, Fe, and Ru. *J. Catal.* **1984**, *87*, 352–362.
186. Sane, S.; Bonnier, J.M.; Damon J.P.; Masson, J. Raney metal catalysts: I. comparative properties of raney nickel proceeding from Ni-Ai intermetallic phases. *Appl. Catal.* **1984**, *9*, 69–83.
187. Lee, G.D.; Moon, M.J.; Park, J.H.; Park, S.S.; Hong, S.S. Raney Ni catalysts derived from different alloy precursors Part II. CO and CO_2 methanation activity. *Korean J. Chem. Eng.* **2005**, *22*, 541–546.
188. Yaccato, K.; Carhart, R.; Hagemeyer, A.; Lesik, A.; Strasser, P.; Volpe, A.F., Jr.; Turner, H.; Weinberg, H.; Grasselli, R.K.; Brooks, C. Competitive CO and CO_2 methanation over supported noble metal catalysts in high throughput scanning mass spectrometer. *Appl. Catal. A* **2005**, *296*, 30–48.
189. Zhang, Y.; Zhang, G.; Wang, L.; Xu, Y.; Sun, Y. Selective methanation of carbon monoxide over Ru-based catalysts in H_2-rich gases. *J. Ind. Eng. Chem.* **2012**, *18*, 1590–1597.
190. Erekson, E.J.; Sughrue, E.L.; Bartholomew, C.H. Catalyst degradation in high temperature methanation. *Fuel Process. Technol.* **1981**, *5*, 91–101.
191. Agnelli, M.; Kolb, M.; Nicot, C.; Mirodatos, C. Sintering of a Ni-based catalyst during CO hydrogenation: Kinetics and modeling. *Stud. Surf. Sci. Catal.* **1991**, *68*, 605–612.
192. Agnelli, M.; Kolb, M.; Mirodatos, C. CO hydrogenation on a nickel catalyst. I. Kinetics and modeling of a low temperature sintering process. *J. Catal.* **1994**, *148*, 9–21.
193. Lu, H.; Yang, X.; Gao, G.; Wang, K.; Shi, Q.; Wang, J.; Han, C.; Liu, J.; Tong, M.; Liang, X.; Li, C. Mesoporous zirconia-modified clays supported nickel catalysts for CO and CO_2 methanation. *Int. J. Hydrog. Energy* **2014**, *39*, 18894–18907.
194. Kodama, T.; Kitayama, Y.; Tsuji, M.; Tamaura, Y. Methanation of CO_2 using ultrafine $Ni_xFe_3–xO_4$. *Energy* **1997**, *22*, 183–187.
195. Ando, H.; Fujiwara, M.; Matsumura, Y.; Miyamura, H.; Souma, Y. Methanation of carbon dioxide over $LaNi_4X$ type catalysts. *Energy Convers. Mgmt.* **1995**, *36*, 653–658.
196. Perkas, N.; Amirian, G.; Zhong, Z.; Teo, J.; Gofer, Y.; Gedanken, A. Methanation of carbon dioxide on Ni catalysts on mesoporous ZrO_2 doped with rare earth oxides. *Catal. Lett*. **2009**, *130*, 455–462.
197. Xavier, K.O.; Streekala, R.; Rashid, K.K.A.; Yusuff, K.K.M.; Sen, B. Doping effects of cerium oxide on Ni/Al_2O_3 catalysts for methanation. *Catal. Today* **1999**, *49*, 17–21.
198. Rynkowski, J.M.; Paryjczak, T.; Lewicki, A.; Szynkowska, M.I.; Maniecki, T.P.; Józwiak, W.K. Characterization of $Ru/CeO_2–Al_2O_3$ catalysts and their performance in CO_2 methanation. *React. Kinet. Catal. Lett.* **2000**, *71*, 55–64.
199. Laosiripojana, N.; Assabumrungrat, S. Methane steam reforming over $Ni/Ce–ZrO_2$ catalyst: Influences of $Ce–ZrO_2$ support on reactivity, resistance toward carbon formation, and intrinsic reaction kinetics. *Appl. Catal. A* **2005**, *290*, 200–211.
200. Monte, R.; Fornasiero, P.; Kaspar, J.; Rumori, P.; Gubitosa, G.; Graziani, M. $Pd/Ce_{0.6}Zr_{0.4}O_2/Al_2O_3$ as advanced materials for three-way catalysts: Part 1. Catalyst characterisation, thermal stability and catalytic activity in the reduction of NO by CO. *Appl. Catal. B* **2000**, *24*,157–167.

201. Abouarnadasse, S.; Pajonk, G.M.; Germain, J.E.; Teichner, S.J. Catalytic nitroxidation of toluene into benzonitrile over nickel oxide-alumina xero- or aero-gel catalysts. *Appl. Catal.* **1984**, *9*, 119–128.
202. Vance, C.K.; Bartholomew, C.H. Hydrogenation of carbon dioxide on group VIII metals: III, Effects of support on activity/selectivity and adsorption properties of nickel. *Appl. Catal.* **1983**, *7* 169–177.
203. Aziz, M.A.A.; Jalil, A.A.; Triwahyono, S.; Mukti, R.R.; Taufiq-Yap, Y.H.; Sazegar, M.R. Highly active Ni-promoted mesostructured silica nanoparticles for CO_2 methanation. *Appl. Catal. B* **2014**, *147*, 359–368.
204. Chen, C.-S.; Lin, J.-H.; Wua, J.-H.; Chiang, C.-Y. Growth of carbon nanofibers synthesized from CO_2 hydrogenation on a K/Ni/Al_2O_3 catalyst. *Catal. Commun.* **2009**, *11*, 220–224.
205. Hwang, S.; Hong, U.G.; Lee, J.; Seo, J.G.; Baik, J.H.; Koh, D.J.; Lim, H.; Song, I.K. Methanation of carbon dioxide over mesoporous Ni–Fe–Al_2O_3 catalysts prepared by a coprecipitation method: Effect of precipitation agent. *J. Ind. Eng. Chem.* **2013**, *19*, 2016–2021.
206. Elliot, D.J.; Lunsford, J.H. Kinetics of the Methanation Reaction over Ru, Ru–Ni, Ru–Cu, and Ni Clusters in Zeolite-Y. *J. Catal.* **1979**, *57*, 11–26.
207. Saha, N.C.; Wolf, E.E. CO methanation activity and XPS studies of Pd supported on ZSM-5 and Y-zeolites. *Appl. Catal.* **1984**, *13*, 101–112.
208. Eckle, S.; Denkwitz, Y.; Behm, R.J. Activity, selectivity, and adsorbed reaction intermediates/reaction side products in the selective methanation of CO in reformate gases on supported Ru catalysts. *J. Catal.* **2010**, *269*, 255–268.
209. Cagnoli, M.V.; Gallegos, N.G.; Alvarez, A.M.; Bengoa, J.F.; Yeramián, A.A.; Schmal, M.; Marchetti, S.G. Catalytic CO hydrogenation on potassic Fe/zeolite LTL. *Appl. Catal. A* **2002**, *230*, 169–176.
210. Abdel-Mageed, A.M.; Eckle, S.; Anfang, H.G.; Behm, R.J. Selective CO methanation in CO_2-rich H_2 atmospheres over a Ru/zeolite catalyst: The influence of catalyst calcination. *J. Catal.* **2013**, *298*, 148–160.
211. Schunemann, V.; Trevino, H.; Lei, G.D.; Tomczack, D.C.; Sachmer, W.M.H.; Fogash, K.; Dumesic, J.A. Fe promoted Rh-clusters in Zeolite NaY: Characterization and catalytic performance in CO hydrogenation. *J. Catal.* **1995**, *153*, 144–157.
212. Scirè, S.; Crisafulli, C.; Maggiore, R.; Minicò, S.; Galvagno, S. Influence of the support on CO_2 methanation over Ru catalysts: An FT-IR study. *Catal. Lett.* **1998**, *51*, 41–45.
213. Patzelová, V.; Zukal, A.; Tvarukova, Z.; Malícek, O. Hydrogenation of CO and CO_2 over stabilized NiY catalysts. *Stud. Surf. Sci. Catal.* **1984**, *18*, 367–374.
214. Eckle, S.; Anfang, H.-G.; Behm, R.J. Reaction intermediates and side products in the methanation of CO and CO_2 over supported Ru catalysts in H_2-rich reformate gases. *J. Phys. Chem. C* **2011**, *115*, 1361–1367.
215. Jwa, E.; Lee, S.B.; Lee, H.W.; Mok, Y.S. Plasma-assisted catalytic methanation of CO and CO_2 over Ni–zeolite catalysts. *Fuel Proc. Technol*. **2013**, *108*, 89–93.
216. Krämer, M.; Stöwe, K.; Duisberg, M.; Müller, F.; Reiser, M.; Sticher, S.; Maier, W.F. The impact of dopants on the activity and selectivity of a Ni-based methanation catalyst. *Appl. Catal. A* **2009**, *369*, 42–52.

217. Men, Y.; Kolb, G.; Zapf, R.; Hessel, V.; Lowe, H. Selective methanation of carbon oxides in a microchannel reactor-primary screening and impact of gas additives. *Catal. Today* **2007**, *125*, 81–87.
218. Ikeue, K.; Yamashita, H.; Anpo, M.; Takewaki, T. Photocatalytic reduction of CO_2 with H_2O on Ti-β zeolite photocatalysts: Effect of the hydrophobic and hydrophilic properties. *J. Phys. Chem. B* **2001**, *105*, 8350–8355.
219. Inoue, T.; Fujishima, A.; Konishi, S.; Honda, K. Photoelectrocatalytic reduction of carbon dioxide in aqueous suspensions of semiconductor powders. *Nature* **1979**, *277*, 637–638.
220. Centi, G.; Perathoner, S. Towards solar fuels from water and CO_2. *ChemSusChem* **2010**, *3*, 195–208.
221. Dhakshinamoorthy, A.; Navalon, S.; Corma, A.; Garcia, H. Photocatalytic CO_2 reduction by TiO_2 and related titanium containing solids. *Energy Environ. Sci.* **2012**, *5*, 9217–9233.
222. Mori, K.; Yamashita, H.; Anpo, M. Photocatalytic reduction of CO_2 with H_2O on various titanium oxide photocatalysts. *RSC Adv.* **2012**, *2*, 3165–3172.
223. Navalón, S.; Dhakshinamoorthy, A.; Álvaro, M.; Garcia, H. Photocatalytic CO_2 reduction using non-titanium metal oxides and sulfides. *ChemSusChem* **2013**, *6*, 562–577.
224. Dvoranova, D.; Brezova, V.; Mazur, M.; Malati, M.A. Investigations of metal-doped titanium dioxide photocatalysts. *Appl. Catal. B* **2002**, *37*, 91–105.
225. Herrmann, J.M. Heterogeneous photocatalysis: Fundamentals and applications to the removal of various types of aqueous pollutants. *Catal. Today* **1999**, *53*, 115–129.
226. Litter, M.I.; Navio, J.A. Photocatalytic properties of iron-doped titania semiconductors photocatalytic properties of iron-doped titania semiconductors. *J. Photochem. Photobiol. A* **1996**, *98*, 171–181.
227. Burda, C.; Lou, Y.B.; Chen, X.B.; Samia, A.C.S.; Stout, J.; Gole, J.L. Enhanced nitrogen doping in TiO_2 nanoparticles. *Nano Lett.* **2003**, *3*, 1049–1051.
228. Yu, J.C.; Ho, W.K.; Yu, J.G.; Yip, H.; Wong, P.K.; Zhao, J.C. Efficient visible-light-induced photocatalytic disinfection on sulfur-doped nanocrystalline titania. *Environ. Sci. Technol*. **2005**, *39*, 1175–1179.
229. Silva, C.G.; Juarez, R.; Marino, T.; Molinari, R.; Garcia, H. Influence of excitation wavelength (UV or visible light) on the photocatalytic activity of titania containing gold nanoparticles for the generation of hydrogen or oxygen from water. *J. Am. Chem. Soc.* **2011**, *133*, 595–602.
230. Primo, A.; Corma, A.; Garcia, H. Titania supported gold nanoparticles as photocatalyst. *Phys. Chem. Chem. Phys.* **2011**, *13*, 886–910.
231. Mul, G.; Schacht, C.; van Swaaij, W.P.M.; Moulijn, J.A. Functioning devices for solar to fuel conversion. *Chem. Eng. Process* **2012**, *51*,137–149.
232. Corma, A.; Garcia, H. Photocatalytic reduction of CO_2 for fuel production: Possibilities and challenges. *J. Catal.* **2013**, *308*, 168–175.
233. Izumi, Y. Recent advances in the photocatalytic conversion of carbon dioxide to fuels with water and/or hydrogen using solar energy and beyond. *Coord. Chem. Rev.* **2013**, *257*, 171–186.
234. Kitano, M.; Matsuoka, M.; Ueshima, M.; Anpo, M. Recent developments in titanium oxide-based photocatalysts. *Appl. Catal. A* **2007**, *325*, 1–14.
235. Matsuoka, M.; Anpo, M.J. Local structures excited states and photocatalytic reactivities of highly dispersed catalysts constructed within zeolites. *J. Photochem. Photobiol. C* **2003**, *3*, 225–252.
236. Usubharatana, P.; McMartin, D.; Veawab, A.; Tontiwachwuthikul, P. Photocatalytic process for CO_2 emission reduction from industrial flue gas streams. *Ind. Eng. Chem. Res.* **2006**, *45*, 2558–2568.

237. Lin, W.; Han, H.; Frei, H. CO_2 splitting by H_2O to CO and O_2 under UV light in TiMCM-41 silicate sieve. *J. Phys. Chem. B* **2004**, *108*, 18269–18273.
238. Tseng, I.-H.; Wu, J.C.S.; Chou, H.-Y. Effects of sol-gel procedures on the photocatalysis of Cu/TiO_2 in CO_2 photoreduction. *J. Catal.* **2004**, *221*, 432–440.
239. Shioya, Y.; Ikeue, K.; Ogawa, M.; Anpo, M. Synthesis of transparent Ti-containing mesoporous silica thin film materials and their unique photocatalytic activity for the reduction of CO_2 with H_2O. *Appl. Catal. A* **2003**, *254*, 251–259.
240. Hori, H.; Koike, K.; Suzuki, Y.; Ishizuka, M.; Tanaka, J.; Takeuchi, K.; Sasaki, Y. High-pressure photocatalytic reduction of carbon dioxide using $[fac\text{-}Re(bpy)(CO)_3P(O^iPr)_3]^+$ (bpy = 2,2'-bipyridine). *J. Mol. Catal. A* **2002**, *179*, 1–9.
241. Ikeue, K.; Nozaki, S.; Ogawa, M.; Anpo, M. Photocatalytic Reduction of CO_2 with H_2O on Ti-containing porous silica thin film photocatalysts. *Catal. Lett.* **2002**, *80*, 111–114.
242. Ikeue, K.; Nozaki, S.; Ogawa, M.; Anpo, M. Characterization of self-standing Ti-containing porous silica thin films and their reactivity for the photocatalytic reduction of CO_2 with H_2O. *Catal. Today* **2002**, *74*, 241–248.
243. Yamashita, H.; Ikeue, K.; Takewaki, T.; Anpo, M. *In situ* XAFS studies on the effects of the hydrophobic–hydrophilic properties of Ti-β zeolites in the photocatalytic reduction of CO_2 with H_2O. *Top. Catal.* **2002**, *18*, 95–100.
244. Saladin, F.; Forss, L.; Kamber, I. Photosynthesis of CH_4 at a TiO_2 surface from gaseous H_2O and CO_2. *J. Chem. Soc. Chem. Commun.* **1995**, 533–534.
245. Anpo, M.; Chiba, K. Photocatalytic reduction of CO_2 on anchored titanium oxide catalysts. *J. Mol. Catal.* **1992**, *74*, 207–212.
246. Anpo, M.; Yamashita, H.; Ichihashi, Y.; Fujii, Y.; Honda, M. Photocatalytic reduction of CO_2 with H_2O on titanium oxides anchored within micropores of zeolites: Effects of the structure of the active sites and the addition of Pt. *J. Phys. Chem. B* **1997**, *101*, 2632–2636.
247. Yamashita, H.; Fujii, Y.; Ichihashi, Y.; Zhang, S.G.; Ikeue, K.; Park, D.R.; Koyano, K.; Tatsumi, T.; Anpo, M. Selective formation of CH_3OH in the photocatalytic reduction of CO_2 with H_2O on titanium oxides highly dispersed within zeolites and mesoporous molecular sieves. *Catal. Today* **1998**, *45*, 221–227.
248. Anpo, M.; Yamashita, H.; Ikeue, K.; Fujii, Y.; Zhang, S.G.; Ichihashi, Y.; Park, D.R.; Suzuki, Y.; Koyano, K.; Tatsumi, T. Photocatalytic reduction of CO_2 with H_2O on Ti–MCM–41 and Ti–MCM–48 mesoporous zeolite catalysts. *Catal. Today* **1998**, *44*, 327–332.
249. Ikeue, K.; Yamashita, H.; Anpo, M. Photocatalytic reduction of CO_2 with H_2O on titanium oxide prepared within the FSM-16 mesoporous zeolites. *Chem. Lett.* **1999**, *11*, 1135–1136.
250. Hwang, J.S.; Chang, J.S.; Park, S.E.; Ikeue, K.; Anpo, M. Photoreduction of carbondioxide on surface functionalized nanoporous catalysts. *Top. Catal.* **2005**, *35*, 311–319.